Monthly Notices
of the
ROYAL ASTRONOMICAL SOCIETY

MNRAS **474,** 197–218 (2018)
Advance Access publication 2017 October 13

doi:10.1093/mnras/stx2668

Supernovae 2016bdu and 2005gl, and their link with SN 2009ip-like transients: another piece of the puzzle

A. Pastorello,[1★] C. S. Kochanek,[2,3] M. Fraser,[4,5†] Subo Dong,[6] N. Elias-Rosa,[1] A. V. Filippenko,[7,8] S. Benetti,[1] E. Cappellaro,[1] L. Tomasella,[1] A. J. Drake,[9] J. Harmanen,[10] T. Reynolds,[10,11] B. J. Shappee,[12‡] S. J. Smartt,[13] K. C. Chambers,[14] M. E. Huber,[14] K. Smith,[13] K. Z. Stanek,[2,3] E. J. Christensen,[15] L. Denneau,[14] S. G. Djorgovski,[9] H. Flewelling,[14] C. Gall,[16,17] A. Gal-Yam,[18] S. Geier,[19,20] A. Heinze,[14] T. W.-S. Holoien,[2,3§] J. Isern,[21] T. Kangas,[10] E. Kankare,[13] R. A. Koff,[22] J.-M. Llapasset,[23] T. B. Lowe,[14] P. Lundqvist,[24] E. A. Magnier,[14] S. Mattila,[10] A. Morales-Garoffolo,[25] R. Mutel,[26] J. Nicolas,[27] P. Ochner,[1,28] E. O. Ofek,[18] E. Prosperi,[29] A. Rest,[30] Y. Sano,[31,32,33] B. Stalder,[14] M. D. Stritzinger,[17] F. Taddia,[24] G. Terreran,[1,13,28] J. L. Tonry,[14] R. J. Wainscoat,[14] C. Waters,[14] H. Weiland,[14] M. Willman,[14] D. R. Young[13] and W. Zheng[7]

Affiliations are listed at the end of the paper

Accepted 2017 October 10. Received 2017 October 10; in original form 2017 April 10

ABSTRACT

Supernova (SN) 2016bdu is an unusual transient resembling SN 2009ip. SN 2009ip-like events are characterized by a long-lasting phase of erratic variability that ends with two luminous outbursts a few weeks apart. The second outburst is significantly more luminous (about 3 mag) than the first. In the case of SN 2016bdu, the first outburst (Event A) reached an absolute magnitude $M_r \approx -15.3$ mag, while the second one (Event B) occurred over one month later and reached $M_r \approx -18$ mag. By inspecting archival data, a faint source at the position of SN 2016bdu is several times in the past few years. We interpret these detections as signatures of a phase of erratic variability, similar to that experienced by SN 2009ip between 2008 and mid-2012, and resembling the currently observed variability of the luminous blue variable SN 2000ch in NGC 3432. Spectroscopic monitoring of SN 2016bdu during the second peak initially shows features typical of an SN IIn. One month after the Event B maximum, the spectra develop broad Balmer lines with P Cygni profiles and broad metal features. At these late phases, the spectra resemble those of a typical Type II SN. All members of this SN 2009ip-like group are remarkably similar to the Type IIn SN 2005gl. For this object, the claim of a terminal SN explosion is supported by the disappearance of the progenitor star. While the similarity with SN 2005gl supports a genuine SN explosion scenario for SN 2009ip-like events, the unequivocal detection of nucleosynthesized elements in their nebular spectra is still missing.

Key words: supernovae: general – supernovae: individual: SN 2016bdu, SN 2005gl, SN 2009ip, SN 2010mc, LSQ13zm, SN 2015bh.

1 INTRODUCTION

While it is well known that many massive stars lose a large fraction of their envelope in the latest stages of their life, the mechanisms that trigger the mass-loss are still poorly understood.

★ E-mail: andrea.pastorello@oapd.inaf.it
† Royal Society – Science Foundation Ireland University Research Fellow.
‡ Hubble Fellow and Carnegie-Princeton Fellow.
§ US Department of Energy Computational Science Graduate Fellow.

Steady winds (Castor, Abbott & Klein 1975; Owocki & Puls 1999; Dwarkadas & Owocki 2002; Lamers & Nugis 2002; Chevalier & Irwin 2011; Moriya et al. 2011; Ginzburg & Balberg 2012), enhanced mass-loss due to binary interaction (Kashi 2010; Kashi & Soker 2010; Smith & Frew 2011; Chevalier 2012; Soker 2012; de Mink et al. 2013; Soker & Kashi 2013), or major outbursts caused by stellar instabilities (Humphreys & Davidson 1994; Langer, García-Segura & Mac Low 1999; Woosley, Blinnikov & Heger 2007; Arnett & Meakin 2011; Chatzopoulos & Wheeler 2012; Moriya & Langer 2014; Shiode & Quataert 2014) can all lead to the formation of extended circumstellar environments (for reviews on this topic, see Langer 2012 and Smith 2014). When stars embedded in such dense cocoons explode as supernovae (SNe), they produce the typical observables of interacting SNe: narrow to intermediate-width lines in emission, a blue spectral continuum, and enhanced X-ray, ultraviolet (UV), and radio fluxes (Weiler et al. 1986; Chugai 1991; Chevalier & Fransson 1994; Filippenko 1997; Aretxaga et al. 1999; Chandra et al. 2012, 2015; Kiewe et al. 2012; Smith et al. 2017). SNe showing spectra with narrow or intermediate-width Balmer lines produced in an H-rich circumstellar medium (CSM) are classified as Type IIn (Schlegel 1990), while those whose spectra are dominated by narrow or intermediate-width He I lines are classified as Type Ibn (Pastorello et al. 2008, 2016; Hosseinzadeh et al. 2017).

Signatures of major instabilities in the last stages of life of very massive stars are frequently observed. These nonterminal eruptions are usually labelled as 'SN impostors' (Van Dyk et al. 2000; Maund et al. 2006). Although they do not necessarily herald terminal SN explosions on short time-scales, such eruptions have been detected from a few weeks to years before the SN in some cases. A seminal case is the Type Ibn SN 2006jc, which had a luminous outburst two years before the final explosion (Foley et al. 2007; Pastorello et al. 2007). Moderate-intensity pre-SN outbursts were also likely observed in more canonical stripped-envelope SNe (Corsi et al. 2014; Strotjohann et al. 2015). More common is the evidence of pre-SN bursts from Type IIn SN progenitors (e.g. Fraser et al. 2013b; Ofek et al. 2014). Pre-SN outbursts were well observed in two Type IIn events: SN 2009ip (Fraser et al. 2013a, 2015; Mauerhan et al. 2013a, 2014; Ofek et al. 2013b; Pastorello et al. 2013a; Smith et al. 2013; Graham et al. 2014, 2017; Margutti et al. 2014; Smith, Andrews & Mauerhan 2016b) and SN 2015bh (Elias-Rosa et al. 2016; Goranskij et al. 2016; Ofek et al. 2016; Thöne et al. 2017). Both sources had historical light curves with signatures of erratic variability over time-scales of years (SN impostor phase), followed by two luminous outbursts separated by a few weeks. In each case, the first outburst (labelled as 'Event A') had an absolute magnitude $M_R \approx -15$ mag, and the second one ('Event B') was brighter, approaching or exceeding $M_R \approx -18$ mag. From a careful inspection of the light curve of SN 2009ip after the Event B maximum, Graham et al. (2014) and Martin et al. (2015) noted luminosity fluctuations consistent with the ejecta colliding with CSM shells produced during the earlier eruptive phase.

Light curves with two outbursts were also observed in SN 2010mc (Ofek et al. 2013a) and LSQ13zm (Tartaglia et al. 2016). These transients were discovered in relatively distant galaxies, and their previous SN-impostor-phase variability would have been too faint to be observed by existing surveys. Two Type IIn events, SNhunt151 (Pastorello et al. 2013b) in UGC 3165 and SN 2016jbu in NGC 2442 (Bose et al. 2017; Fraser et al. 2017), exhibited double-outburst light curves, and evidence of the progenitor's variability in previous years (Elias-Rosa et al. 2017; Kilpatrick et al. 2017). A pre-SN outburst and a complex, bumpy light curve were also observed in the Type IIn SN iPTF13z (Nyholm et al. 2017). In addition, OGLE-2014-SN-173 and SN 2016cvk were proposed as SN 2009ip-like candidates (Walton et al. 2015; Brown et al. 2016).

Even accounting for these recent discoveries, pre-SN outbursts have been directly detected only occasionally. Nonetheless, based on the Palomar Transient Factory (PTF) sample control time and coadding images in multiple-day bins to go deeper than the nominal limiting magnitude of the survey, Ofek et al. (2014) claim that these events are quite frequent, but in most cases below the detection threshold of individual pre-explosion images. This likely explains the lack of precursor outburst detections in the sample of SNe IIn of the Katzman Automatic Imaging Telescope survey (Bilinski et al. 2015).

Some authors (e.g. Pastorello et al. 2013a; Thöne et al. 2017) have noted the resemblance of the impostor phase of SNe 2009ip and 2015bh to the erratic variability exhibited by the SN impostor NGC3432-LBV1 (also known as SN 2000ch; Wagner et al. 2004; Pastorello et al. 2010) over the last two decades. This is in fact an excellent candidate to become another SN 2009ip analogue, perhaps within a human lifetime.

In this context, a new SN 2009ip-like event is important for improving our understanding of these unusual explosions. SN 2016bdu was discovered on 2016 May 24.43 UT (JD = 245 7532.93; UT dates are used throughout this paper) by the PanSTARRS-1 (PS1) Survey for Transients (PSST)[1] (Huber et al. 2015; Chambers et al. 2016) at $\alpha = 13^{\rm h}10^{\rm m}13\overset{\rm s}{.}95$, $\delta = +32^{\circ}31'14\overset{''}{.}07$ (J2000.0). The SN candidate exploded in the very faint ($g = 21.19$, $r = 20.94$ mag) galaxy SDSS J131014.04+323115.9. The SN is clearly offset by 2.1 arcsec from the centre of its host in the PS1 images. The All-Sky Automated Survey for Supernovae (ASAS-SN; Shappee et al. 2014) detected the object again on 2016 May 29.38, and soon thereafter it was classified by the 2.56 m Nordic Optical telescope (NOT) Unbiased Transient Survey (NUTS)[2] collaboration (Mattila et al. 2016) as a Type IIn SN (Terreran et al. 2016a).

Terreran et al. (2016a) noted that the transient was offset by 2.6 arcmin (hence about 57 kpc) from the centre of a relatively large, edge-on spiral galaxy, UGC 08250. This galaxy has a redshift $z = 0.0176$ (Courtois & Tully 2015; Garcia-Benito et al. 2015). For $H_0 = 73\,{\rm km\,s^{-1}\,Mpc^{-1}}$, $\Omega_{\rm M} = 0.27$, and $\Omega_\Lambda = 0.73$, the luminosity distance of $d_L = 73.3$ Mpc and the distance modulus of $\mu = 34.33$ mag. If we correct for Local Group infall into Virgo ($v_{\rm Vir} = 5474\,{\rm km\,s^{-1}}$), we infer a slightly larger luminosity distance of $d_{L,{\rm Vir}} = 76.1$ Mpc ($\mu_{\rm Vir} = 34.41$ mag). We will assume that the faint host of SN 2016bdu (SDSS J131014.04+323115.9) is associated with UGC 08250 (see Fig. 1). From the position of the peaks of the most prominent narrow emission lines in the transient's spectra, we estimate the redshift of SDSS J131014.04+323115.9 to be $z = 0.0173 \pm 0.0002$ ($d_L = 72.0$ Mpc and $\mu = 34.29$ mag), consistent with this association. We adopt the Virgo-infall-corrected distance modulus for this redshift of $\mu_{\rm Vir} = 34.37 \pm 0.15$ mag.

The nondetection of the interstellar Na I doublet (Na I D) absorption lines at the redshift of SDSS J131014.04+323115.9 suggests that there is negligible reddening due to the host galaxy; hence, we adopt only the Milky Way contribution $E(B-V) = 0.013$ mag (Schlafly & Finkbeiner 2011) as the total interstellar extinction towards SN 2016bdu. Given these distance and reddening estimates, SDSS J131014.04+323115.9 has a total absolute magnitude $M_g = -13.23$ mag, and an intrinsic colour of $g - r = 0.23$ mag. This makes the galaxy hosting SN 2016bdu much less luminous

[1] Oddly, the temporary PSST name, PS16bdu, recalled the final International Astronomical Union designation.
[2] http://csp2.lco.cl/not/.

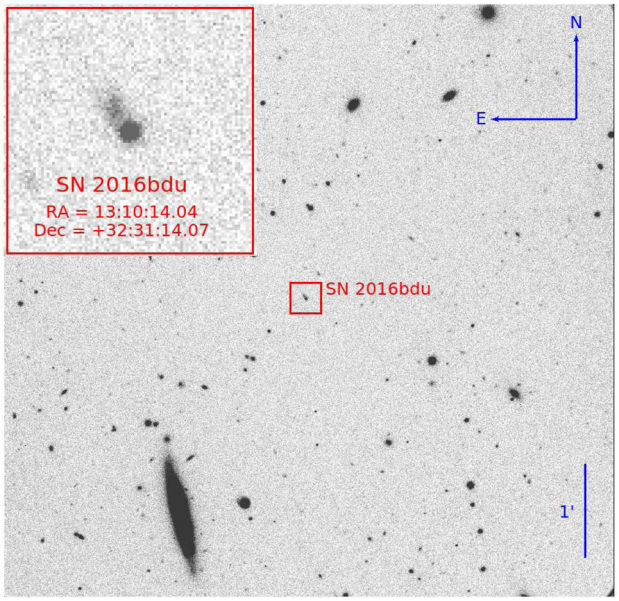

Figure 1. SN 2016bdu and the surrounding stellar field. The large, edge-on spiral galaxy visible in the bottom-left corner is UGC 08250. Sloan *r*-band image taken on 2016 February 29 with the NOT and the ALFOSC camera. A detail showing the host galaxy and the SN is in the upper-left corner.

than the Magellanic Clouds, possibly suggesting that SN 2016bdu exploded in a low-metallicity environment.

The structure of this paper is as follows. In Section 2, we present photometric and spectroscopic observations of SN 2016bdu, Section 3 discusses plausible scenarios to explain the sequence of outbursts experienced by the SN 2016bdu progenitor, and a summary follows in Section 4.

2 OBSERVATIONS

Soon after the discovery, our inspection of archival images revealed that the pre-discovery photometric evolution of the stellar precursor of SN 2016bdu resembled that of SN 2009ip. For this reason, we decided to initiate an extensive follow-up campaign in the optical and near-infrared (NIR) domains.

The optical and NIR data were obtained with the NOT using ALFOSC and NOTCam, the 2.0 m Liverpool Telescope (LT) using IO:O, the 10.4 m Gran Telescopio Canarias (GTC) using OSIRIS, the 1.82 m Copernico Telescope using AFOSC, and the 1.5 m Tillinghast Telescope using the FAST spectrograph. Additional photometry was obtained using a Meade 10 arcsec LX-200 Schmidt–Cassegrain Telescope with an Apogee AP-47 CCD camera located near Bennett (Colorado, USA), and the 0.51 m Iowa Robotic Telescope of the Winer Observatory (in southern Arizona, USA), equipped with a cooled, back-illuminated 1024 × 1024 pixel CCD sensor. Further photometry (including archival data) was later provided by ASAS-SN[3] (Shappee et al. 2014), PSST[4] (Huber et al. 2015), the Catalina Real-Time Transient Survey[5] (CRTS; Drake et al. 2009; Djorgovski et al. 2012), and the Asteroid Terrestrial-impact Last Alert System (ATLAS)[6]. Additional *R*-band data were provided by the PTF second data release (Law et al. 2009; Ofek et al. 2012), from the Infrared Processing and Analysis Center[7] (Laher et al. 2014). Finally, a few photometric epochs from 1998 to 2003 calibrated in the Johnson–Bessell *V*-band magnitude scale were obtained from images taken by the Near Earth Asteroid Tracking (NEAT) programme, and retrieved through the SkyMorph GSFC website.[8]

2.1 Photometry

The science images were first reduced using IRAF.[9] These preliminary operations included overscan, bias, and flat-field corrections, for both imaging and spectroscopy. The magnitudes of SN 2016bdu were measured using a dedicated package (SNOoPY; Cappellaro 2014) that performs point-spread-function (PSF) fitting photometry on the original or the template-subtracted images. Since the SN field falls in the sky area mapped by the Sloan Digital Sky Survey (SDSS), we identified a sequence of reference stars, and measured nightly zero-points and instrumental colour terms. These were used to accurately calibrate the SN magnitudes on the different nights. The Johnson–Bessell *B* and *V* magnitudes of the reference stars were computed from the Sloan magnitudes following the relations of Chonis & Gaskell (2008). PTF *R*-band data were converted to the Sloan *r*-band photometric system using magnitudes of comparison stars taken from the SDSS catalogue, while unfiltered data were scaled to Sloan *r*-band magnitudes. NIR images from NOTCam were reduced using a slightly modified version of the IRAF package NOTCam v.2.5,[10] and photometric measurements were performed after the subtraction of the luminous NIR sky. The instrumental SN magnitudes were calibrated using the 2MASS catalogue (Skrutskie et al. 2006). Final SN magnitudes are listed in Tables A1, A2, and A3 of Appendix A.

As shown in Fig. 2, the light curve of SN 2016bdu has two main brightening events, similar to other SN 2009ip-like transients. In analogy with the labelling adopted for SN 2009ip (Pastorello et al. 2013a), the nonmonotonic brightening observed in the light curve from about four months before the discovery of SN 2016bdu is named Event A. We note that Event A of SN 2009ip is different, having a much shorter duration and a monotonic rise to the maximum. In SN 2016bdu, Event A reaches a peak of $r = 19.1 \pm 0.2$ mag (on JD = 245 7509 ±6, obtained through a low-order polynomial fit) in about three months. Then the luminosity slightly declines to $r = 19.44 \pm 0.25$ mag, before rising again to the second peak (Event B) that is reached about one month later (on JD = 245 7541.5 ±1.5). The maximum magnitude of Event B is $r = 16.37 \pm 0.03$ mag. The *V*-band peak of Event B is reached on JD = 245 7540.9 ± 1.8, with $V = 16.46 \pm 0.03$ mag. After maximum, the light curve declines rapidly for about one month, more slowly between days 30 and 60 past-peak, and finally the decline rate increases again during

[3] The survey uses four 14 cm 'Brutus' robotic telescopes located in the Haleakala station (Hawaii, USA) of the Las Cumbres Observatory Global Telescope (LCOGT) network.
[4] PSST uses the PS1-1.8 m telescope (Chambers et al. 2016), which has a 7 deg^2 field of view, with a mosaic CCD camera, operating on Haleakala in the island of Maui, Hawaii, USA.
[5] The survey uses the 0.7 m Schmidt Telescope of the Bigelow Station, and has an archive covering about 13 yr of observations.
[6] This survey uses two 0.5 m wide-field telescopes on Mauna Loa and Haleakala in Hawaii, USA (Tonry 2011), one of which is operational.
[7] http://www.ipac.caltech.edu/; the PTF survey used the 1.2 m Oschin Telescope at Palomar Observatory equipped with a 7.8 deg^2 CCD array (CFH12K).
[8] http://skyview.gsfc.nasa.gov/skymorph/skymorph.html
[9] IRAF is distributed by the National Optical Astronomy Observatory, which is operated by the Association of Universities for Research in Astronomy under a cooperative agreement with the National Science Foundation.
[10] http://www.not.iac.es/instruments/notcam/guide/observe.html#reductions

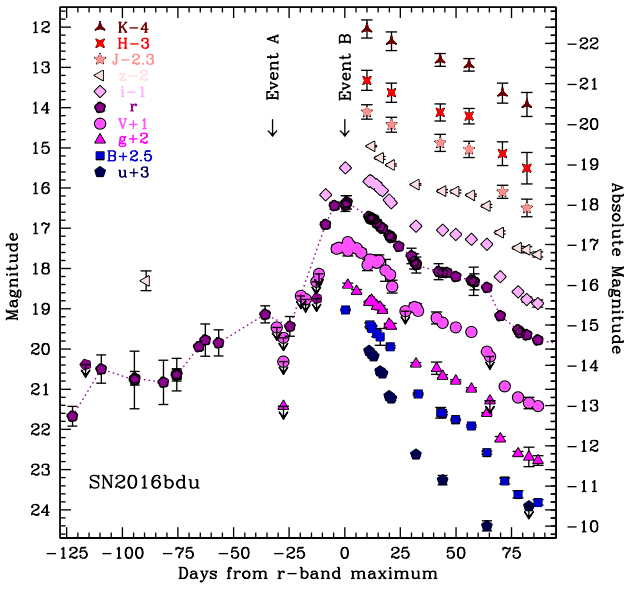

Figure 2. Multi-band light curves of SN 2016bdu. The most recent pre-discovery observations are also shown. The phases are computed with respect to the Sloan *r*-band maximum of Event B (JD = 245 7541.5; see the text). The epochs of the peaks of Events A and B are indicated. The *BVJHK* data are in the Vega magnitude system, and the Sloan *ugriz* data are in the AB magnitude system. The dotted line connects *r*-band data, and reveals fluctuations in the light curve during Event A and in the post-peak decline from Event B.

the last month covered by our photometric campaign. This trend is observed both in the optical and NIR bands. As mentioned before, low-contrast undulations are observed in all bands during Event A (see Fig. 2), and when the light curve declines after the peak of Event B. Similar behaviour was observed in SN 2009ip (Graham et al. 2014; Martin et al. 2015) and interpreted as signatures of ejecta colliding with previously ejected circumstellar shells.

In this context, it is worth noting that some sparse detections of a source at the position of SN 2016bdu have occurred over a period of several years before the SN (see Table A2). A few marginal detections in CRTS images are registered from 2005 to 2008. We note that they are 0.3–0.5 mag brighter than the host-galaxy magnitude ($r = 20.94$ mag; this is fainter than the typical detection limits of individual CRTS images). A source is also visible near the SN position in 2009 April–June, although the magnitudes in the PTF images ($r \approx 21.1$–21.3 mag) are consistent (within the uncertainties) with that of the host galaxy. From about four years before the SN discovery, there is a set of clear detections, with the source well resolved in the host galaxy in several PS1 images: in 2012 January–April ($r = 20.20 \pm 0.25$ mag), March 2014 ($g = 21.63 \pm 0.17$, $i = 21.44 \pm 0.29$ mag), and 2015 April–May ($r = 20.1 \pm 0.4$ mag). Finally, there are repeated detections, starting in 2016 January, before the rise to the Event A peak. The pre-discovery data are shown in Fig. 3. Unfortunately, in most images collected from CRTS, the source is below the instrumental detection threshold. However, the object is detected in the deeper PS1 and PTF images, indicating that the object was in outburst (with absolute magnitude M_R ranging from −13 to −14 mag), and was characterized by erratic variability. The peak magnitudes of these pre-discovery images of SN 2016bdu are comparable with those of the brightest outbursts of

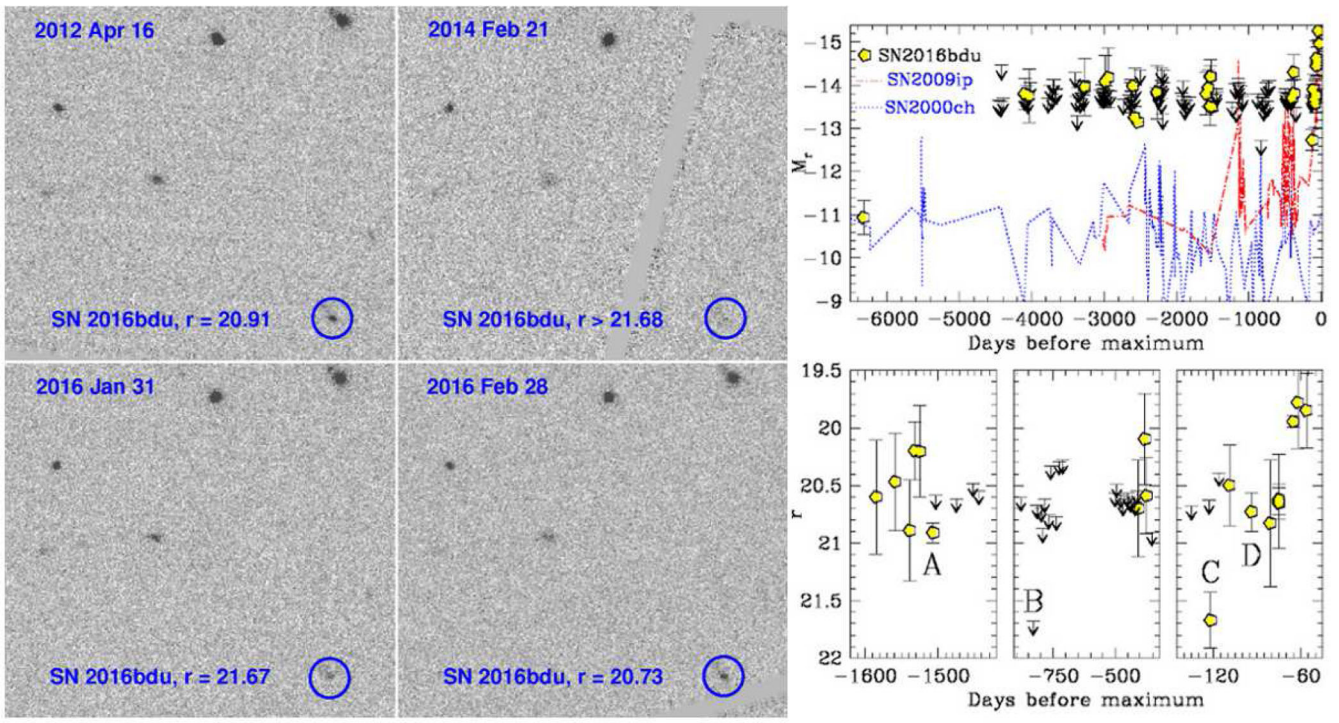

Figure 3. Left-hand panel: pre-discovery Sloan *r*-band images of the location of SN 2016bdu obtained with PS1 on 2012 April 16 (top left, A), 2014 February 21 (top right, B), 2016 January 31 (bottom left, C), 2016 February 28 (bottom right, D), with the transient being at different luminosities. Right-hand panel, top: comparison of the pre-discovery absolute *r*-band light curve of SN 2016bdu with the *R*-band light curves of the impostor SN 2000ch and the pre-explosion variability of SN 2009ip. Right-hand panel, bottom: *r*-band magnitude variability of the transient in SDSS J131014.04+323115.9 before its discovery. The magnitudes corresponding to the images on the left are marked with uppercase letters.

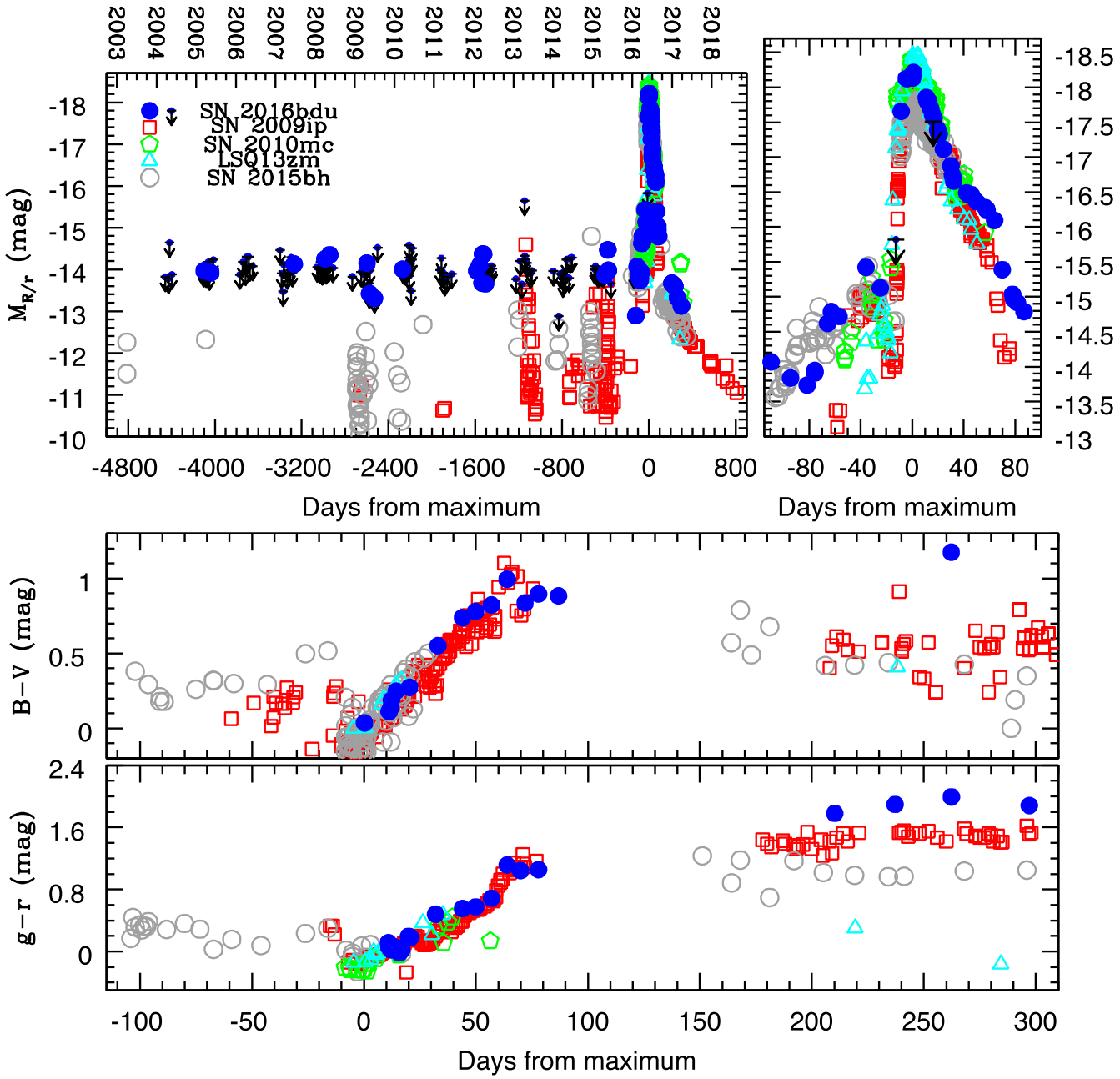

Figure 4. Johnson–Cousins *R* or Sloan *r* absolute magnitude light curves for our sample of SN 2009ip-like events, spanning 15 yr (top left), and during the period encompassing the Events A and B (top right). For clarity, pre-discovery detection limits are shown only for SN 2016bdu. These limits were obtained by placing an artificial star close to the position of SN 2016bdu with a typical signal-to-noise ratio (S/N) of 1.5–2.5. The years above the top-left panel refer to the evolution of SN 2016bdu. $B - V$ (middle) and $g - r$ (bottom) colour evolution for SN 2009ip-like SNe. The phases are in days from the Event B peak.

SN 2009ip during the impostor phase (years 2010–2012; Mauerhan et al. 2013a; Pastorello et al. 2013a, see also the top-right panel in Fig. 3). However, because of the larger distance of SN 2016bdu and the limited depth of most of the archival images, we generally have only upper limits on the source flux in the low-luminosity states between the outbursts.

In Fig. 4, we compare the *r*-band absolute magnitude light curve of SN 2016bdu to those of SN 2009ip (Smith et al. 2010; Fraser et al. 2013a, 2015; Mauerhan et al. 2013a; Pastorello et al. 2013a; Prieto et al. 2013; Graham et al. 2014; Margutti et al. 2014; Martin et al. 2015), SN 2010mc (Ofek et al. 2013a), LSQ13zm (Tartaglia et al. 2016), and SN 2015bh (Goranskij et al. 2016; Elias-Rosa et al. 2016; Ofek et al. 2016; Thöne et al. 2017). If Sloan-*r* data are not available, the Johnson–Cousins *R*-band light curves are shown. For homogeneity, all data have been transformed to the Vega system. The data for SN 2009ip, SN 2010mc, and LSQ13zm are corrected for Milky Way reddening. For SN 2015bh, we adopt the total reddening estimate of $E(B - V) = 0.21$ mag from Thöne et al. (2017). In the top-left panel, in particular, we show the long-term photometric evolution of our SN sample over a temporal window of almost 15 yr. A close-up view including the rise to Event A and the decline after the peak of Event B is shown in the top-right panel. The photometric evolution is surprisingly similar for all objects in this sample. In particular, we note the following.

(i) There are occasional detections in the 'impostor phase' from weeks to years before the onset of Event A in at least three objects: SN 2009ip, SN 2015bh, and SN 2016bdu. For the two other objects, we speculate that the impostor phase remained undetected because of the larger distances to their host galaxies.

(ii) The duration of Event A appears to vary for the five objects, lasting from a few weeks in LSQ13zm (Tartaglia et al. 2016) to over 3 months, and with a bumpy rise in SN 2016bdu and SN 2015bh (Elias-Rosa et al. 2016; Thöne et al. 2017). The absolute magnitudes of the A events are between $M_{R/r} = -14.5$ and -15.3 mag.

(iii) All objects show a relatively fast rise to the Event B maximum ($M_{r/R} \leq -18$ mag) followed by a relatively steep decline. Some undulations in the light curve of SN 2009ip are observed (Martin et al. 2015), and a nonlinear decline is also detected in SN 2016bdu.

(iv) When late-time observations are available, the light curves have flattened, with decline rates slower than the ^{56}Co decay and without any clear evidence of further light-curve fluctuations (Margutti et al. 2014; Fraser et al. 2015; Elias-Rosa et al. 2016; Thöne et al. 2017).

The bottom panel of Fig. 4 shows the $B - V$ and $g - r$ colours. Again, the evolution of the two colours is similar for all the objects from day -20 (from the peak of Event B) to day $+80$. In particular, the colours become bluer from day -20 to day 0, with $B - V$ ranging from -0.5 to 0 mag, and $g - r$ from 0.3 to -0.2 mag. Later on, from day 0 to 80, the colours become redder, spanning from $B - V = 0$ to 1.1 mag and $g - r = -0.2$ to 1.2 mag. More dispersion in the colour evolution is observed at later phases, especially in $g - r$, although large uncertainties affect the photometric measurements at these epochs. Nonetheless, the $g - r$ colour of SN 2016bdu is the reddest in the sample, being about 2 mag at ∼8 months after maximum brightness.

2.2 Quasi-bolometric light curve

Using the available optical photometry of SN 2016bdu, we obtain a quasi-bolometric light curve by integrating the extinction-corrected fluxes at each epoch with the trapezoidal rule. We assume zero flux at the integration extremes. We also estimate a quasi-bolometric light curve including the NIR data when they are available. Since no NIR data are available for SN 2016bdu before the Event B peak, we compute the optical+NIR light curve only for later phases. The resulting quasi-bolometric light curves are shown in Fig. 5. These curves are compared to those obtained for the best-studied example, SN 2009ip. For SN 2009ip, we show results for the optical bands only, optical plus NIR, and the *uvoir* (from the UV to the NIR domain). The similarity of the two objects is striking. In addition, the available data for SN 2016bdu suggest a late-time decline of its quasi-bolometric luminosity that is slightly flatter than the rate expected from the radioactive decay of ^{56}Co into ^{56}Fe. This suggests that the ejecta-CSM interaction is still the dominant mechanism powering the light curve of both SNe at very late phases. This claim will be discussed further in Section 2.3.

For SN 2016bdu, the NIR contributes up to 20 per cent of the total luminosity budget at the Event B maximum, rising to about 30 per cent at the late phases (∼8 months later). The missing UV contribution in SN 2016bdu can be estimated by assuming that it is similar to that of SN 2009ip, where the UV contribution is large (nearly 50 per cent) at the time of the Event B peak, and negligible (<5 per cent) at the late phases.

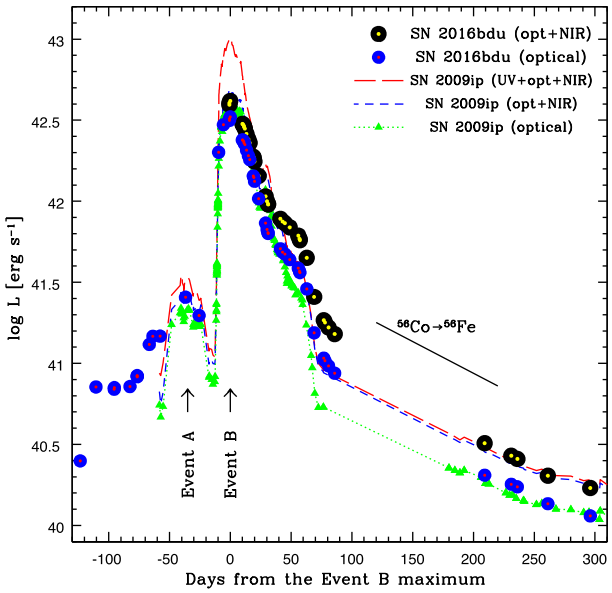

Figure 5. Quasi-bolometric light curves of SNe 2016bdu and 2009ip. For SN 2016bdu, the curves obtained by integrating the optical bands only are shown as small blue–red points, and those including the NIR contribution are shown as large black–yellow points. For SN 2009ip, we show the optical curve (green dotted line), the optical plus NIR curve (blue, short-dashed line), and the *uvoir* curve (see the text; red long-dashed line).

2.3 Spectroscopy

Our extensive spectroscopic campaign for SN 2016bdu started on 2016 June 2, near the Event B light-curve peak. General information on the spectra is collected in Table 1.[11] Most of the spectra were taken at the parallactic angle (Filippenko 1982), hence minimizing differential flux losses.

The spectra were reduced with IRAF tasks.[12] One-dimensional spectra were first extracted from the two-dimensional frames, and then wavelength-calibrated using spectra of comparison lamps obtained with the same instrumental setup. The wavelength calibration was checked by measuring the positions of several night-sky lines, and (when necessary) shifted by a constant amount to match the expected wavelength of these lines. The flux calibration was performed using spectra of standard stars obtained during the same night as the SN observation, and the accuracy of the calibration was checked with the available coeval photometry; in cases of an overall flux discrepancy, a scaling factor was applied to calibrate the spectrum to the photometry. Finally, the strongest telluric absorption bands (in particular, O_2 and H_2O) were corrected using the spectra of the standard stars.

The spectral sequence obtained during the first ∼80 d after the Event B maximum is shown in the top panel of Fig. 6, while line identifications in our earliest spectrum (phase +1 d) are reported in the bottom panel of Fig. 6. The detailed evolution of the Hα and Hβ line profiles is shown in Fig. 7.

The early-time spectra resemble those of typical Type IIn SNe, and are characterized by a blue continuum (with a blackbody

[11] All of our spectra will be available in the WISeREP archive (Yaron & Gal-Yam 2012).

[12] AFOSC and ALFOSC spectroscopic data were reduced using a dedicated graphic user interface developed by E. Cappellaro (http://sngroup.oapd.inaf.it/foscgui.html).

Table 1. Spectroscopic observations of SN 2016bdu. Phases calculated from Sloan *r*-band max of Event B (JD = 245 7541.5).

Date	JD	Phase (d)	Instrumental config.	Range (Å)	FWHM (Å)
2016-06-02	245 7542.49	1.0	NOT + ALFOSC + gm4	3500–9700	14
2016-06-03	245 7542.68	1.2	Tillinghast + FAST + 300tr	3500–7400	6
2016-06-14	245 7553.55	12.1	NOT + ALFOSC + gm4	3500–9700	18
2016-06-17	245 7557.37	15.9	1.82 m Copernico + AFOSC + VPH7 + VPH6	3350–9300	14 and 15
2016-06-22	245 7562.39	20.9	1.82 m Copernico + AFOSC + VPH7 + VPH6	3500–9300	14 and 15
2016-07-02	245 7571.51	30.0	NOT + ALFOSC + gm4	3400–9700	14
2016-07-15	245 7585.45	44.0	NOT + ALFOSC + gm4	3400–9650	18
2016-07-17	245 7587.43	45.9	GTC + OSIRIS + R1000B + R1000R	3650–9350	7 and 8
2016-07-29	245 7599.46	58.0	NOT + ALFOSC + gm4	3400–9700	14
2016-08-12	245 7613.41	71.9	TNG + LRS + LRB	3500–8000	14
2016-08-19	245 7620.38	78.9	GTC + OSIRIS + R1000R	5100–9600	8
2017-01-17	245 7770.73	229.2	GTC + OSIRIS + R1000R	5100–9300	8
2017-01-20	245 7773.68	232.2	GTC + OSIRIS + R1000B + R1000R	3700–10 100	7 and 8

temperature $T_{\rm BB} = 17\,000 \pm 1000$ K) and narrow emission lines of H and He I. These lines show two velocity components: a narrow component with a full width at half-maximum intensity (FWHM) velocity of $v_{\rm FWHM} = 400\,{\rm km\,s^{-1}}$ (as determined from the highest resolution FAST spectrum obtained on June 3) superposed on lower intensity, broader P Cygni wings. In analogy with classical SNe IIn, the narrow emission lines likely arise in a slow-moving, unshocked photoionized CSM, while the broader wings can be interpreted as being produced by electron scattering. The broad P Cygni minimum of Hβ is blueshifted by $v = 3400\,{\rm km\,s^{-1}}$ (see Fig. 7). This value is consistent with that derived from the position of the minimum of the He I λ5876 absorption line.

With time, the spectral continuum becomes redder, and the narrow components weaken relative to the broad emission lines. In particular, when the continuum has declined to $T_{\rm BB} = 13\,500 \pm 1100$ K in the June 14 spectrum (phase +12.1 d), narrow He I lines are no longer visible. The broad He I λ5876 feature displays a P Cygni profile whose velocity (from the position of the absorption minimum) is $v \approx 9000\,{\rm km\,s^{-1}}$. A similar broad P Cygni component is also visible for the H lines, with Hα having $v = 9500\,{\rm km\,s^{-1}}$ and Hβ at $v = 8400\,{\rm km\,s^{-1}}$ (Fig. 7), with blueshifted absorption wings extending up to $13\,000\,{\rm km\,s^{-1}}$. These velocities are likely representative of the fast-moving ejecta. The narrow H components are still visible, and exhibit a P Cygni profile, with the absorption component being blueshifted by about $1900\,{\rm km\,s^{-1}}$ (as measured for the Hβ line).

A possible explanation for the evolution of the Hβ absorption trough (Fig. 7) is the presence of a fast shell close to the SN, produced by a stellar wind with a mass-loss rate of $\sim 10^{-1}\,{\rm M_\odot\,yr^{-1}}$. This interpretation, proposed by Chugai et al. (2004) and Dessart et al. (2014) for the Type IIn SN 1994W, can also work for the early-time spectra of SN 2016bdu. The interaction between the massive SN ejecta with this wind produces a dense shell, which initially has a velocity of $3400\,{\rm km\,s^{-1}}$ and, later on, slows down to $1900\,{\rm km\,s^{-1}}$.

On July 2 (phase 30 d), the spectrum of SN 2016bdu becomes redder ($T_{\rm BB} = 9300 \pm 1100$ K), and the broad absorption components of the Balmer lines are now more prominent. The narrow components of the H features are still visible, with the P Cygni profiles blueshifted by about $1200\,{\rm km\,s^{-1}}$. This velocity, which will stay roughly constant at later phases, is likely very close to the initial velocity of the shell. The He I λ5876 line remains quite weak, and its very broad, boxy absorption profile suggests some contamination from a growing Na I $\lambda\lambda$5890, 5896 doublet (Na I D). An alternative explanation for this line profile is an additional absorption contribution from an He-rich shell. At this epoch, the line velocities inferred for the broad Hα and Hβ absorptions are $v = 7300\,{\rm km\,s^{-1}}$ and $v = 6800\,{\rm km\,s^{-1}}$, respectively. Some Fe II lines (in particular, those of the multiplet 42) are also barely detected.

Later on, from July 15 (phase 44 d), the now quite red ($T_{\rm BB} = 6100 \pm 800$ K) spectrum develops relatively broad lines of metals in absorption, including several Fe II multiplets, Na I D, and Ca II. O I λ7774 is also marginally detected. The Na I D feature now dominates over He I λ5876, while other He,I lines are no longer observed.

On July 29 (58 d), we obtained a high-S/N spectrum that shows a blackbody temperature similar to the one at 44 d. The SN spectrum is still dominated by broad lines with P Cygni profiles. Numerous metal lines are strong, including Fe II (with average $v = 2800\,{\rm km\,s^{-1}}$), Na I D ($v = 3700\,{\rm km\,s^{-1}}$), Ca II H&K, and the (weak) NIR triplet of Ca II. The broad P Cygni lines of the Balmer series are prominent, with the residual narrow H components being detectable only in Hα and Hβ. The gas velocities, as estimated from the minima of the broad Balmer absorptions, are $v = 6700\,{\rm km\,s^{-1}}$ and $v = 5450\,{\rm km\,s^{-1}}$ for Hα and Hβ, respectively (Fig. 7). A prominent feature is also detected blueward of Na I D, at about 5600 Å; we tentatively identify it as Sc II. Finally, Ti II lines very likely contribute to the blanketing at blue wavelengths.

Late-time spectra were obtained on August 12 and August 19 (phases 71.9 d and 78.9 d, respectively). The spectrum has now significantly changed. The continuum is very weak, and the H lines are dominated by the broader component in emission. There are still detectable narrow components superposed on the broad lines. The unblended He I λ7065 feature becomes visible again (and relatively prominent), with $v_{\rm FWHM} = 2800\,{\rm km\,s^{-1}}$, along with an Na I D plus He I λ5876 blend, with a residual P Cygni profile (the absorption minimum is blueshifted by about $3800\,{\rm km\,s^{-1}}$). A weak emission line at about 7200 Å is probably the emerging [Ca II] doublet (possibly blended with He I λ7281), and the NIR Ca II triplet is now prominent. A broad and weak feature appearing at about 6300 Å could be a signature of the growing [O I] $\lambda\lambda$6300, 6364 doublet.

When the object was visible again in 2017 mid-January (phase $\sim$230 d) after the seasonal gap, we obtained two additional spectra with GTC+OSIRIS (Fig. 8). The spectra do not show major changes from those obtained in 2016 August, although the residual P Cygni absorption features have now completely vanished. The overall Hα line profile and the increased strength of He I lines suggest that SN 2016bdu is still interacting with its CSM, although some broad features expected in SN spectra during the nebular phase are now

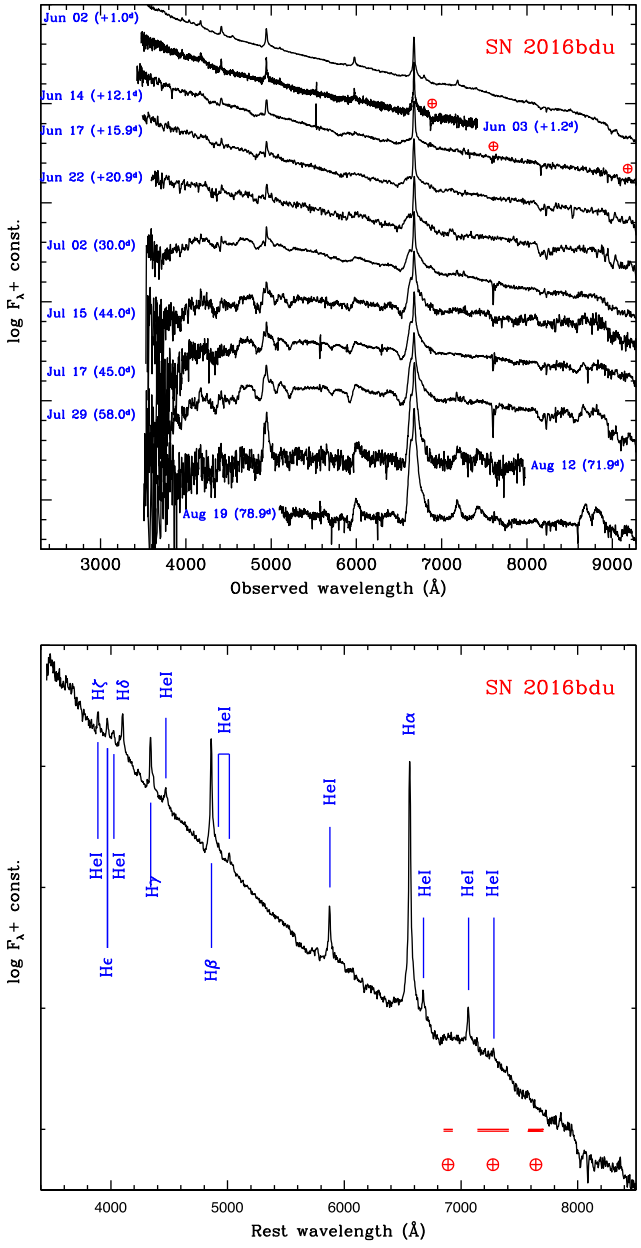

Figure 6. Top: spectroscopic evolution of SN 2016bdu from around the epoch of the Event B maximum (JD = 245 7541.5), to the early nebular phase (+78.9 d). Bottom: identification of the strongest emission lines in the earliest SN 2016bdu spectrum. The regions contaminated by the strongest telluric bands are marked.

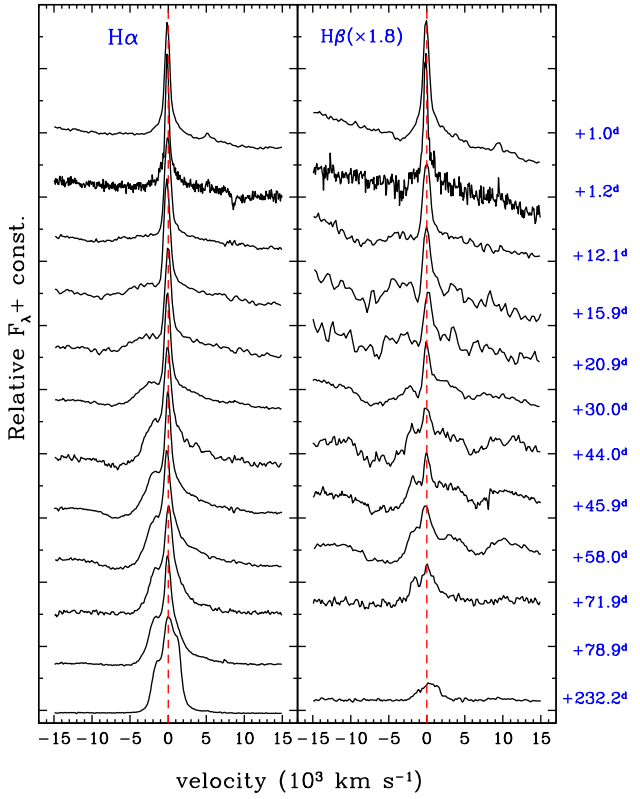

Figure 7. Evolution of the Hα (left-hand panel) and Hβ (right-hand panel) line profiles in velocity space. The vertical red dashed lines mark the rest-velocity position of the two lines.

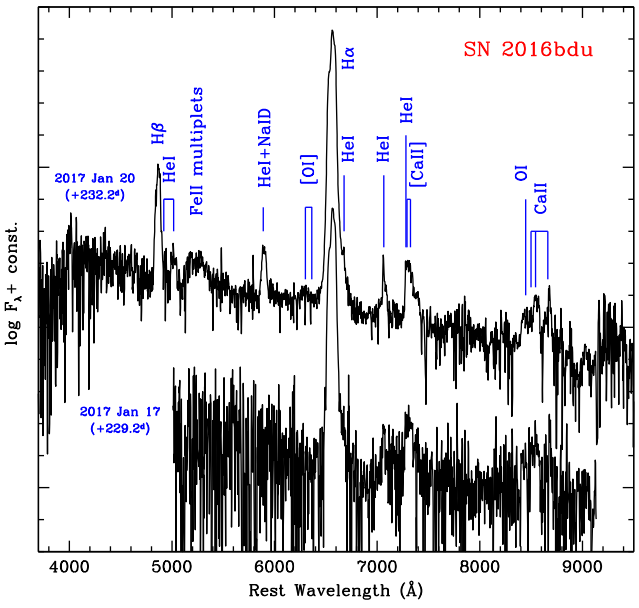

Figure 8. Late-time (∼200–230 d) GTC+OSIRIS spectra of SN 2016bdu, along with identifications of the most prominent lines.

clearly detected. The nebular lines (in particular [O I], [Ca II], and NIR Ca II) are still much fainter than Hα. Hβ is also detected, along with a number of He I lines. Comprehensive line identifications for the two latest spectra are given in Fig. 8.

The Hα FWHM in our latest spectra exceeds 3000 km s^{-1}, and the line has an asymmetric profile, with two shoulders: one blueshifted by about 1250 km s^{-1}, the other redshifted by nearly 900 km s^{-1} (Fig. 7). Although asymmetric Balmer line profiles are usually interpreted as signatures of asymmetric material ejection, the overall line shape of the H lines can be most likely explained as boxy profiles with a superimposed narrow P Cygni component from the CSM. We also measure an Hα/Hβ line ratio (Balmer decrement) of 11. Such large Balmer decrements are quite common in SNe IIn (e.g. SNe 1995G and 1996al; Pastorello et al. 2002; Benetti et al. 2016), and are frequently viewed as indicative of collisional excitation (Branch et al. 1981). An alternative explanation for the asymmetric Balmer line profiles and the large Balmer decrement could be that some dust is forming and is obscuring the receding material. However, this interpretation seems less

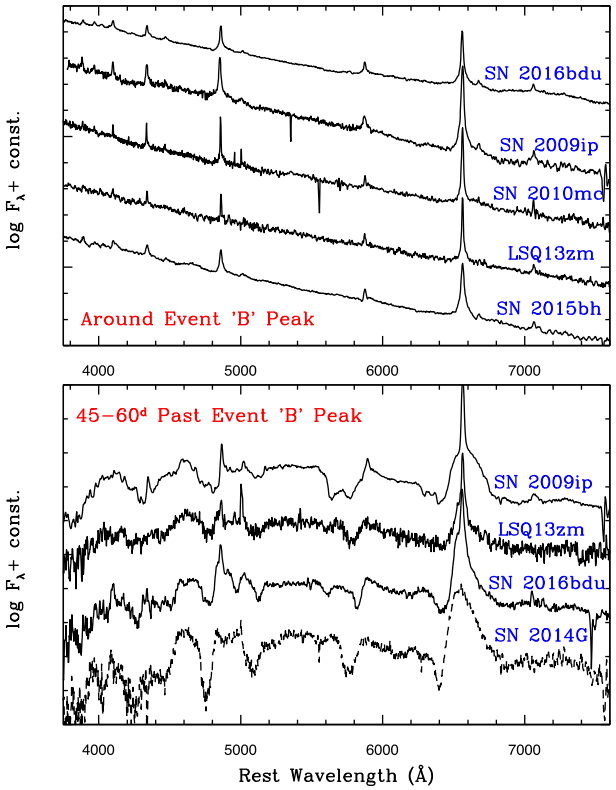

Figure 9. Top: comparison of spectra of SN 2009ip-like events obtained around the epoch of the Event B maximum (the spectra are from Ofek et al. 2013a; Graham et al. 2014; Elias-Rosa et al. 2016; Tartaglia et al. 2016). Bottom: comparison of spectra of SNe 2009ip (Fraser et al. 2013a), LSQ13zm (Tartaglia et al. 2016), and 2016bdu with a spectrum of the more typical Type II SN 2014G (Terreran et al. 2016b).

plausible, as there is no evidence of an NIR excess in our late-time photometry.

While the early-time spectra of SN 2016bdu (around the Event B maximum) are very similar to those of other SN 2009ip-like transients at the same phase (see Fig. 9, top panel), later spectra of SN 2016bdu closely resemble those of typical SNe II during the early H-envelope recombination phase (Fig. 9, bottom panel). This supports the argument for a terminal SN explosion for all SN 2009ip-like objects, although this claim is still debated since broad lines were also detected in pre-SN stages in some cases (e.g. Pastorello et al. 2013a). The different scenarios proposed for SN 2009ip, revised in the context of SN 2016bdu, will be discussed in Section 3.

3 ERUPTIONS, MERGERS, OR SN EXPLOSIONS?

As mentioned earlier, at least three SNe of this family have experienced a phase of major erratic variability lasting several years prior to the primary outburst, but the actual number is likely much larger. For example, in the more distant LSQ13zm and SN 2010mc, the earlier phase of erratic variability was probably below the detection threshold. All five objects experienced a major outburst, characterized by a light curve showing two brightening episodes. The duration and the luminosity of the two events are comparable in all SN 2009ip-like objects, which also show remarkable similarity in their spectral evolution (at least, at phases when spectroscopic observations exist; see Section 2.3). This observed homogeneity is even more puzzling for progenitors possessing strongly asymmetric circumstellar environments (Levesque et al. 2014; Mauerhan et al. 2014; Elias-Rosa et al. 2016; Thöne et al. 2017), whose orientation with respect to the line of sight is expected to play an important role. The striking spectroscopic and photometric similarities of the five SN 2009ip-like transients suggest that these objects very likely arise from similar stars (or stellar systems) and may have undergone a comparable fate.

The nature of SN 2009ip and similar objects has been widely discussed in the literature, and multiple scenarios have been offered, none of them supported by conclusive evidence. In this section, we discuss the most plausible scenarios for these peculiar transients.

(i) **A major outburst (Event A) followed by shell–shell collision (Event B).** This scenario was first proposed by Pastorello et al. (2013a) for SN 2009ip. The argument was based on the evidence that broad spectral lines, with velocities comparable with those of real SNe, were observed during the 2008 to early-2012 impostor phase of SN 2009ip, long before the putative SN. In this view, Event A in July 2012, whose spectra showed broad P Cygni lines, would be a huge outburst, with the subsequent Event B being the result of reprocessing of kinetic energy into radiation due to collision of the most recent mass ejection (Event A) with CSM collected during previous eruptive phases. This scenario is also supported by the lack of late-time nebular SN spectral signatures expected from the explosion of a massive star (Fraser et al. 2013a, 2015; Graham et al. 2014; Margutti et al. 2014). Based on energetic considerations, Moriya (2015) suggested that Event B in SN 2009ip was not caused by the interaction of material expelled in a regular SN explosion with CSM, but rather from a shell–shell interaction. The mechanisms that trigger these major mass-loss events are debated, and plausible explanations invoke pulsational pair-instability (e.g. Woosley et al. 2007), or interactions in a massive binary system (e.g. Kashi & Soker 2010). This latter scenario was also suggested for the impostor SN 2000ch (Pastorello et al. 2010).

An argument frequently used to rule out a terminal SN explosion is the absence of emission lines from nucleosynthetic byproducts in the late-time spectra of these objects (see e.g. the discussion in Fraser et al. 2015, for SN 2009ip). The late-time spectrum of the SN 2009ip-like event SN 2015bh, in fact, exhibits prominent and relatively broad (about 3000 km s^{-1}) [Ca II] λλ7291, 7324 lines, but does not show unequivocal evidence of the broad [O I] λλ6300, 6364 features expected from a classical core-collapse SN. The [Ca II] λλ7291, 7324 emission is not necessarily a tracer of freshly nucleosynthesized elements, as it can be produced by primordial material.

One of the key observational constraints for our understanding of SN 2009ip-like transients is the flattening of the late-time light curve observed in SN 2009ip, LSQ13zm, and SN 2015bh at phases later than 150–200 d. A flattening in the late-time light curve is also observed for SN 2016bdu. Although the spectral appearance in this phase suggests CSM interaction is still playing a key role, the exponential luminosity decline without significant variability may indicate that the progenitors have returned to a quiescent phase or eventually disappeared after core collapse. Although none of the above arguments is conclusive, the scenario invoking an outburst followed by shell–shell collisions appears to be less appealing.

(ii) **A faint core-collapse SN (Event A) plus ejecta-CSM interaction (Event B).** This scenario for explaining the double-peaked light curve of the SN 2009ip-like transients was first proposed by Mauerhan et al. (2013a) for SN 2009ip, and expanded by Smith, Mauerhan & Prieto (2014) who also suggested that the ∼60 M$_\odot$ progenitor was a blue supergiant that exploded as a faint core-collapse SN during Event A. Such massive stars may, in fact,

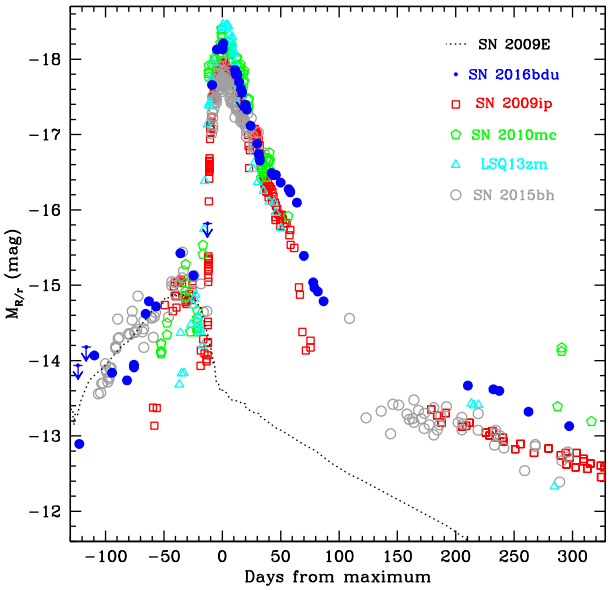

Figure 10. Comparison of Johnson–Cousins *R* (or Sloan-*r*) absolute light curves for our sample of SN 2009ip-like events with the light curve of the faintest known SN 1987A-like SN 2009E (Pastorello et al. 2012). All data are on the Vega magnitude scale. The phases span from the maximum of Event B to the late-time ^{56}Co decay tail. The light curve of SN 2009E has been shifted arbitrarily in phase to approximately match the Event A peaks of SN 2009ip-like SNe, and has been dimmed by 1 mag.

produce underenergetic (10^{50} erg) explosions, and eject very little ^{56}Ni owing to fallback on to the protoneutron star (Zampieri, Shapiro & Colpi 1998; Heger et al. 2003; Nomoto et al. 2006; Moriya et al. 2010; Pejcha & Thompson 2015; Sukhbold et al. 2016). The result is a weak core-collapse SN, consistent with the properties of Event A. A fallback SN (producing the Event A light curve) would also explain the weakness of the α-element signatures in late-time spectra. The subsequent collision of the outer SN ejecta with the CSM from the more recent mass-loss events produces the major rebrightening during Event B (see e.g. Chugai 1991). This scenario is also supported by a sequence of spectropolarimetric observations of SN 2009ip; these data suggest that SN 2009ip Event A is consistent with a prolate (possibly bipolar) SN explosion having a canonical kinetic energy ($E_K \approx 10^{51}$ erg), and whose ejecta collide with an oblate CSM distribution (Mauerhan et al. 2014).

A similar scenario has been invoked by Elias-Rosa et al. (2016) for SN 2015bh based on the surprising similarity between the light curve of SN 2015bh during Event A and weak SN 1987A-like events (e.g. SN 2009E; see Fig. 10; Pastorello et al. 2012). The light curve of SN 2016bdu during Event A is consistent with a faint core-collapse SN (perhaps SN 1987A-like; Fig. 10).

This scenario was not favoured by Ofek et al. (2013a) for SN 2010mc on the basis of the following arguments. The impact of SN ejecta with the CSM generates collisionless shocks, which produce hard X-ray photons (Chevalier 2012; Svirski, Nakar & Sari 2012). To reprocess these photons to visible light through Compton scattering, an optical depth on the order of a few times unity is necessary. Using the temperature and the emitting radius estimated from blackbody fits to the spectral continuum of SN 2010mc, Ofek et al. (2013a) inferred that (for the assumed optical depths) the diffusion time-scales were longer than the observed duration of the Event A peak of SN 2010mc. On the other hand, all the other transients of this group (including SN 2016bdu) have much longer rise times to the Event A peak than does SN 2010mc. In addition, an asymmetric gas distribution as observed in both SNe 2009ip and 2015bh (e.g. Levesque et al. 2014; Mauerhan et al. 2014; Elias-Rosa et al. 2016) may weaken the Ofek et al. arguments.

(iii) **An outburst (Event A) followed by an interacting SN explosion (Event B).** In this scenario, Event A would be the last and most energetic outburst of a sequence likely initiated a few years before (during the impostor phase). Then, the rise of Event B would be the direct signature of the true SN explosion. The blue spectra, characterized by prominent, narrow emission lines of H and He I, would be produced in the CSM, initially photoionized by the SN shock breakout and later by the CSM-ejecta interaction. This scenario was first proposed for SN 2010mc (Ofek et al. 2013a) and a few other SNe IIn in the PTF sample (Ofek et al. 2014). It was also suggested by Tartaglia et al. (2016) to explain the very high velocities (2.3×10^4 km s^{-1}) observed in spectra of LSQ13zm. In fact, when adopting for LSQ13zm the epoch of the initial rise of Event A as the time of the SN shock breakout, a photospheric velocity of more than 2×10^4 km s^{-1} would be observed ∼70 d after the SN explosion, which is unusual in typical core-collapse SNe. We also note that the spectra of LSQ13zm ∼50 d after the Event B maximum are reminiscent of SN II spectra during the photospheric phase (bottom panel of Fig. 9). Moving up the epoch of core collapse to the onset of Event A (i.e. at least 3 months before the peak of Event B) would imply that the H-envelope recombination phase occurs rather late (4–5 months after the explosion). A similar sequence of events was also proposed for the pre-SN outburst of a Wolf–Rayet star two years before the explosion of the Type Ibn SN 2006jc (Foley et al. 2007; Pastorello et al. 2007), and the outburst of a putative super-asymptotic-giant-branch star was observed a few months before the explosion of the Type IIn-P SN 2011ht (possibly an electron-capture SN; Fraser et al. 2013b; Mauerhan et al. 2013b; Smith 2013). However, other authors suggest that the properties of SNe IIn-P are best explained as resulting from the interaction of subsequent shells produced by two nonterminal outbursts (Dessart et al. 2009; Humphreys et al. 2012).

(iv) **Binary interaction during Event A (and before) with a final merger (Event B).** The possibility that SN 2009ip-like events are produced in interacting binary systems has been previously mentioned. This would be consistent with pre-SN histories characterized by erratic variability and a multiple-shell CSM structure (Pastorello et al. 2013a; Graham et al. 2014; Margutti et al. 2014; Martin et al. 2015). In addition, Levesque et al. (2014) constrained the geometry of the SN 2009ip CSM to have an accretion disc (see also Mauerhan et al. 2014). All of this suggests the presence of a companion star in a highly eccentric orbit, with interactions between the two stars during each periastron passage triggering ejections of material.

Kashi, Soker & Moskovitz (2013) proposed that Event B in SN 2009ip was powered by the accretion of several solar masses of gas on to the primary luminous blue variable (LBV) star. The secondary star may have survived the encounter or eventually merged on to the primary. This scenario has also been suggested by Soker & Kashi (2013) and Soker & Kashi (2016) for SNe 2009ip, 2010mc, and 2015bh (see also Sana et al. 2012; de Mink et al. 2014; Justham, Podsiadlowski & Vink 2014; Portegies Zwart & van den Heuvel 2016, for a discussion of massive stellar mergers including LBVs). In these massive binary systems, formed by an LBV and a more compact companion, the high-velocity gas outflow seen in the spectra of both SN 2009ip and SN 2015bh during the impostor phase (hence months to years before Event A) would be powered by jets from the secondary star (Tsebrenko & Soker 2013). Goranskij et al. (2016) proposed a hybrid explanation for SN 2015bh, with the core collapse of an evolved massive star while merging with a

massive binary companion. In this context, we note that some bumps similar to those observed in SN 2009ip are also visible in the light curve of SN 2016bdu during the rise to the Event A maximum, and during the post-peak decline from Event B.

Although binary interaction followed by a merging event cannot be definitely ruled out for SN 2016bdu, there are additional arguments that do not support this scenario. First, the spectra of the most promising merger candidates seem to evolve towards those of cool, M-type stars (e.g. Smith et al. 2016a; Blagorodnova et al. 2017), which is obviously not the case for SN 2009ip-like events. Secondly, all known stellar mergers follow clear correlations between the physical parameters of the progenitors and the luminosity of the outbursts (Kochanek, Adams & Belczynski 2014). The known high-mass mergers also follow these correlations (Mauerhan et al. 2017, and references therein), while the SN 2009ip-like transients are much more luminous for their expected stellar masses.

In summary, SN 2016bdu is observationally a member of the SN 2009ip-like family. Although none of the alternative scenarios is ruled out, the spectroscopic features observed during the decline following Event B closely resemble those of rather normal SNe II, favouring a terminal core-collapse explosion for SN 2016bdu (and, plausibly, for all members of this family). Whether core collapse happened at the onset of Event A or B is also controversial. Further clues supporting the terminal SN explosion for SN 2016bdu and all other clones of SN 2009ip will be provided from the comparison with the well-studied Type IIn SN 2005gl, below.

3.1 SN 2005gl: a link with SN 2009ip-like events?

Important insights on the nature of SN 2016bdu may come from a comparison with the Type IIn SN 2005gl, an object sharing some similarity with SN 2009ip-like events, and for which a very luminous source at the position of the SN was identified in pre-SN *Hubble Space Telescope* (*HST*) archival images obtained in 1997 June. This object was interpreted by Gal-Yam et al. (2007) as the probable SN progenitor. In particular, late-time observations of the site of SN 2005gl showed no trace of the putative progenitor (Gal-Yam & Leonard 2009), which provides support for the correct identification of the progenitor and direct evidence that a massive star, very likely an LBV, exploded to produce an SN IIn. Identifying SN 2005gl as a member of the SN 2009ip-like family would provide reasonable arguments to claim that all members of this family experienced a similar fate.

Here, we provide a few observational arguments to support the similarity of SN 2005gl with members of the SN 2009ip group. In Fig. 11, we compare spectra of SN 2005gl (Gal-Yam et al. 2007) at three representative epochs with those of SNe 2009ip and 2016bdu at similar phases (indicated by labels in the figure). The striking spectral similarity of SN 2005gl with the SN 2009ip-like events is evident both around maximum brightness and at later phases. The observed behaviour of these objects differs from that of classical SNe IIn (Schlegel 1990),[13] whose optical luminosities are expected to decline more slowly, and their slow-evolving spectra are usually dominated by narrow and intermediate-width emission lines, without broad P Cygni profiles.

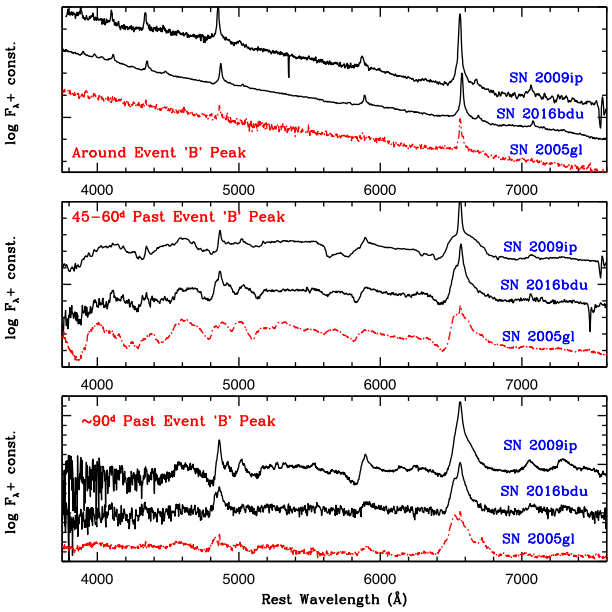

Figure 11. Comparison of the spectra of SNe 2009ip, 2016bdu, and 2005gl obtained at three epochs around the Event B maximum (top), 1.5–2 months after the Event B maximum (middle), and about 3 months after the Event B maximum (bottom). The spectra of SNe 2005gl and 2009ip are taken from Gal-Yam et al. (2007); Fraser et al. (2013a); Graham et al. (2014) and Margutti et al. (2014).

We also compute an updated light curve of SN 2005gl from follow-up photometry obtained with the 0.76 m Katzman Automatic Imaging Telescope (KAIT, at Lick Observatory; Filippenko et al. 2001; Leaman et al. 2011), along with new unfiltered observations from amateur astronomers calibrated to the *R* band (details are given in Appendix B, and the photometric measurements are reported in Table B1).

In the top panel of Fig. 12, a close-up view of SN 2005gl and SNe 2009ip, 2015bh, and 2016bdu during their Events A/B is shown. A good match is also seen between the light curve of SN 2005gl and those of SN 2009ip-like transients during their Event B. SN 2005gl reaches an absolute peak magnitude $M_R \approx -17.6$, which is very close to (just marginally fainter than) that of our SN sample, In addition, the light curves of SN 2005gl and the SN 2009ip-like transients are quite similar, and evolve more rapidly than those of most SNe IIn.

Despite the similarity of the Event B light curves, there is no robust detection of an Event A in SN 2005gl down to an absolute magnitude of about −13.7. There is a single marginal detection with S/N = 2.7 ($M_R = -14.46$ mag) about 90 d before the light-curve maximum of SN 2005gl. It is unclear if this is a signature of a short-duration outburst, or a hot pixel accidentally located at the transient's position. The magnitude of this possible precursor is brighter than most of the detection limits measured in the subsequent ∼50 d.

In order to address whether SN 2005gl also had an erratic-variability impostor phase and a previously unseen Event A, we analysed the KAIT images of the host galaxy of SN 2005gl prior to the outburst (1998 October to 2005 July) using the template-subtraction technique, stacking the images to increase their depth. The template was obtained by median combining a large number of good-quality KAIT images obtained between 2007 and 2009, since we are confident there is no contamination from SN 2005gl or

[13] Objects like SN 1998S (Fassia et al. 2000, 2001; Fransson et al. 2005) and SN 2008fq (Taddia et al. 2013) are also classified as SNe IIn. However, they are somewhat transitional events, sharing a few observational similarities with the objects discussed in this paper, but without showing the broad Hα absorption component. Unfortunately, both of them were discovered close to the maximum light; hence, we do not have information on their earlier evolution.

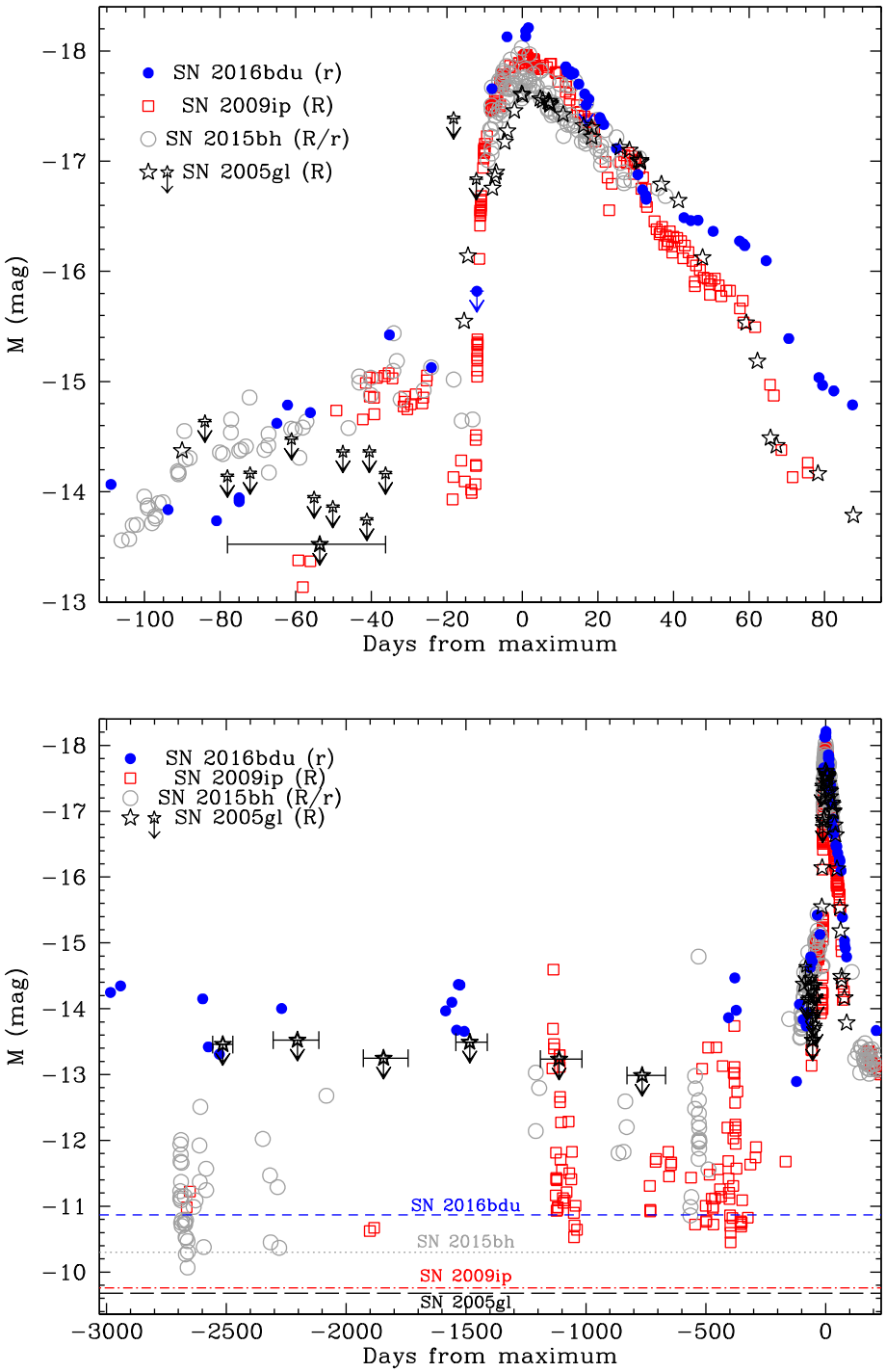

Figure 12. Top: comparison of the absolute Johnson–Cousins *R*-band and Sloan *r*-band light curves of SNe 2005gl, 2016bdu, 2009ip (Fraser et al. 2013a; Pastorello et al. 2013a), and 2015bh (Elias-Rosa et al. 2016) in the Vega magnitude system. The phase covered is that of the main outburst. Photometric points of SN 2005gl with horizontal error bars represent detection limits inferred from seasonal stacked images. Bottom: long-term absolute Johnson–Cousins *R*-band and/or Sloan *r*-band light curves of SNe 2005gl, 2016bdu, 2009ip (Fraser et al. 2013a; Pastorello et al. 2013a; Prieto et al. 2013; Margutti et al. 2014), and 2015bh (Elias-Rosa et al. 2016). While for SN 2005gl, the detection limits are also reported, for all other events we show only real detections. The distance modulus of SN 2009ip is taken from Fraser et al. (2013a), while we revised that of SN 2005gl to $\mu = 34.11$ mag. For the line-of-sight extinction in the direction of SN 2005gl, we adopt the upper limit ($E(B - V) = 0.1$ mag) reported by Gal-Yam et al. (2007). The faintest archival detections for the progenitors of SN 2016bdu (short-dashed blue line), SN 2009ip (dot–dashed red line), SN 2015bh (dotted grey line), and SN 2005gl (long-dashed black line) are also indicated. Except for SN 2016bdu, for which the weakest pre-outburst detection is in the Sloan *r* band, all other pre-outburst sources were detected in archival *HST* images in *F*547*W*, *F*555*W*, or *F*606*W*, which can be approximated by the *V* band.

its progenitor at these epochs. In fact, Gal-Yam & Leonard (2009) found no signature of a source at the SN location in deep *HST* images obtained on 2007 September, to a 2σ limit of $V > 25.9$ mag. The long-term R-band light curve of SN 2005gl (including the deep detection limits obtained from seasonal stacked images) is compared with those of our sample of SN 2009ip-like transients during their impostor phases in the bottom panel of Fig. 12. Unfortunately, after the template subtraction, there is no evidence of pre-SN outbursts brighter than $M_R \approx -13$ to -13.5 mag over this time period (Fig. 12, bottom panel). While this limit is fainter than the variability observed for SN 2016bdu, many of the SN 2009ip-like events showed pre-Event A variability at only moderately fainter luminosities; thus, it is possible that SN 2005gl did so as well.

The observational match of SN 2005gl with SN 2009ip-like transients suggests a close link between all of these objects, and it may have important implications on the interpretation of their nature. The progenitor candidate identified by Gal-Yam et al. (2007) and Gal-Yam & Leonard (2009) had $V = 24.1 \pm 0.2$ mag, implying an absolute magnitude of $M_V \approx -9.7$. This source was extremely luminous, and was consistent with being an LBV (Gal-Yam & Leonard 2009). Whether this LBV was in a quiescent stage or in an eruptive phase is uncertain, as there was only one detection in a single band.

We also inspected ground-based archival images of the field of SN 2016bdu, and found a source with $r = 23.46 \pm 0.39$ mag in very deep Isaac Newton Telescope (INT) images taken on 1999 February 10. To our knowledge, this is the faintest detection available of a stellar source at the position of SN 2016bdu. Owing to the relatively low spatial resolution of the image, this source can be either the variable progenitor of SN 2016bdu, a blend of multiple objects, or even an unrelated background source. No detection was registered in Johnson–Bessell V and Sloan i images collected on 1998 June 19 to a limit of $V > 23.78$ and $i > 23.65$ mag. We note that the progenitors of other SN 2009ip-like events have been observed in archival *HST* images, and have absolute V-band magnitudes quite close to -10 mag (Smith et al. 2010; Foley et al. 2011; Elias-Rosa et al. 2016). These faint progenitor detections are indicated with horizontal lines in Fig. 12.

Since post-explosion *HST* images indicate that the stellar source detected by Gal-Yam et al. (2007) at the position of SN 2005gl is now below the *HST* detection threshold (Gal-Yam & Leonard 2009), this implies that the star finally exploded as a SN or, alternatively, the surviving star is much fainter than the 1997 June detection.

So far, we do not have unequivocal proof that any of the SN 2009ip-like transients are associated with terminal SN explosions. Although the spectra obtained during Event A, and at 1–3 months after the maximum of Event B, show features closely resembling those of typical SNe II, late-time follow-up observations of SN 2009ip (over 3 yr after the peak of Event B) show only marginal evidence of the classical nebular features of a core-collapse SN (e.g. the prominent forbidden lines of O I and Ca II expected in the explosion of massive stars; see Fraser et al. 2015, and references therein). However, the late-time photometric evolution of this object (but also, for example, that of SN 2015bh) is slower than the expected decay rate of ^{56}Co, without any signature of the photometric fluctuations observed during past evolutionary stages. This evolution is consistent with that of a genuine SN interacting with its CSM. More importantly, SN 2009ip is still fading, and it now has a magnitude comparable with that of the pre-explosion progenitor (Smith et al. 2016b), making the terminal explosion scenario plausible for this event. If future observations demonstrate the disappearance of SN 2009ip-like transients, their similarity with SN 2005gl along with the observational clues mentioned above provide an additional argument for the death of their progenitor stars, as suggested by several authors (Mauerhan et al. 2013a, 2014; Smith et al. 2014; Elias-Rosa et al. 2016; Tartaglia et al. 2016).

4 SUMMARY

In this paper, we presented optical and NIR observations of the recent Type IIn SN 2016bdu, along with additional optical photometric data for SN 2005gl. There is a striking observational match among SN 2016bdu, SN 2009ip, and other similar transients, as follows.

(i) Most have a pre-SN impostor phase characterized by an erratically variable light curve, similar to what is currently observed for the impostor SN 2000ch (Wagner et al. 2004; Pastorello et al. 2010).
(ii) They have two sequential luminous outbursts (Events A and B) with similar structures.
(iii) There is a dramatic decline of the luminosity after the maximum of Event B, followed by a flattening of the late-time light curve to a decline rate slower than that expected from ^{56}Co decay into ^{56}Fe.

Although we have no spectra of SN 2016bdu during Event A, we note that the spectroscopic evolution during Event B is remarkably homogeneous as well:

(i) At maximum brightness, their spectra are blue and show narrow emission lines of H and He I, similar to those observed in the spectra of young SNe IIn.
(ii) During the steep post-peak decline (1–2 months after maximum), the spectra develop broad P Cygni lines of H and metals, becoming similar to those of noninteracting (or mildly interacting) Type II SNe.
(iii) Finally, at late phases (when the light curve flattens), the dominant spectral features are intermediate-width Balmer emission lines, with asymmetric profiles, likely indicative of enhanced ejecta-CSM interaction. The asymmetric Hα line profile may also indicate asymmetries in the gas distribution or, less likely, dust formation.

We also note the striking similarity of SN 2016bdu and other SN 2009ip-like transients with the Type IIn SN 2005gl, although in the latter we did not find unequivocal evidence of an Event A. SN 2005gl is the first interacting SN whose LBV progenitor was identified in pre-explosion images and not recovered in post-explosion images (Gal-Yam & Leonard 2009), indicating that the star had finally exploded as a SN.

Late-time observations might provide new insights into the nature of SN 2016bdu and similar objects through the detection of spectral signatures of a core-collapse SN remnant, or the disappearance of their progenitor stars. Nonetheless, the surprising similarity of the spectra after the Event B maximum with those of more typical SNe II, and the excellent observational match with the SN IIn 2005gl, provide support for the terminal SN explosion scenario for SN 2016bdu and all members of the SN 2009ip-like family.

ACKNOWLEDGEMENTS

We acknowledge S. Ascenzi, S. B. Cenko, R. Kotak, P. E. Nugent, N. Primak, A. S. B. Schultz, D. E. Wright, S. Yang for their contribution to the observations and useful suggestions, and Y. Cai for reading the paper before submission. AP, NER, SB, and GT are partially supported by the PRIN-INAF 2014 with the project 'Transient Universe: unveiling new types of stellar explosions with PESSTO.' NER acknowledges financial support by MIUR PRIN 2010-2011, 'The dark Universe and the cosmic evolution of baryons: from current

surveys to Euclid.' MF acknowledges the support of a Royal Society – Science Foundation Ireland University Research Fellowship. This work is partly supported by the European Union FP7 programme through ERC grant number 320360. KZS and CSK are supported by US National Science Foundation (NSF) grants AST-1515876 and AST-1515927. SD is supported by Project 11573003 supported by NSFC and the 'Strategic Priority Research Program - The Emergence of Cosmological Structures' of the Chinese Academy of Sciences (Grant No. XDB09000000). BJS is supported by the National Aeronautics and Space Administration (NASA) through Hubble Fellowship grant HST-HF-51348.001 awarded by the Space Telescope Science Institute (STScI), which is operated by the Association of Universities for Research in Astronomy, Inc. (AURA) under NASA contract NAS 5-26555. AVF and WZ are grateful for financial assistance from NSF grant AST-1211916, the TABASGO Foundation, the Christopher R. Redlich Fund, and the Miller Institute for Basic Research in Science (U.C. Berkeley); they also acknowledge support through grant HST-AR-14295 from STScI, which is operated by AURA under NASA contract NAS 5-26555. The work of AVF was conducted in part at the Aspen Center for Physics, which is supported by NSF grant PHY-1607611; he thanks the Center for its hospitality during the neutron stars workshop in 2017 June and July. TW-SH is supported by the DOE Computational Science Graduate Fellowship, grant number DE-FG02-97ER25308. Support for J.L.P. is in part by FONDECYT through the grant 1151445 and by the Ministry of Economy, Development, and Tourism's Millennium Science Initiative through grant IC120009, awarded to The Millennium Institute of Astrophysics, MAS. SJS acknowledges (FP7/2007-2013)/ERCgrant 291222. TK acknowledges financial support by the Emil Aaltonen Foundation. JH acknowledges financial support from the Finnish Cultural Foundation and the Vilho, Yrjö and Kalle Väisälä Foundation of the Finnish Academy of Science and Letters. AG-Y is supported by the EU/FP7 via ERCgrant No. 307260, the Quantum Universe I-Core program by the Israeli Committee for Planning and Budgeting, and the ISF; and by a Kimmel award. EOO is grateful to support by grants Israel Science Foundation, Minerva, and the I-CORE Program of the Planning and Budgeting Committee and The Israel Science Foundation. MS acknowledges generous funding from the Danish Agency for Science and Technology and Innovation realized through a Sapere Aude Level II grant, and from the Villum foundation.

The CRTS survey is supported by NSF grants AST-1313422 and AST-1413600. ATLAS observations were supported by NASA grantNN12AR55G. NUTS is supported in part by the Instrument Center for Danish Astrophysics (IDA). We thank Las Cumbres Observatory and its staff for their continued support of ASAS-SN. ASAS-SN is funded in part by the Gordon and Betty Moore Foundation through grant GBMF5490 to the Ohio State University, NSF grant AST-1515927, the Center for Cosmology and AstroParticle Physics (CCAPP) at OSU, the Chinese Academy of Sciences South America Center for Astronomy (CASSACA), the Mt Cuba Astronomical Foundation, and George Skestos.

The Pan-STARRS1 Surveys (PS1) have been made possible through contributions of the Institute for Astronomy, the University of Hawaii, the Pan-STARRS Project Office, the Max-Planck Society and its participating institutes, the Max Planck Institute for Astronomy, Heidelberg and the Max Planck Institute for Extraterrestrial Physics, Garching, The Johns Hopkins University, Durham University, the University of Edinburgh, Queen's University Belfast, the Harvard-Smithsonian Center for Astrophysics, the Las Cumbres Observatory Global Telescope Network Incorporated, the National Central University of Taiwan, STScI, NASA under Grant No. NNX08AR22G issued through the Planetary Science Division of the NASA Science Mission Directorate, the US NSF under Grant No. AST-1238877, the University of Maryland, and Eotvos Lorand University (ELTE). Operation of the Pan-STARRS1 telescope is supported by NASA under Grant No. NNX12AR65G and Grant No. NNX14AM74G issued through the NEO Observation Program.

This work is based in part on observations made with the Nordic Optical Telescope (NOT), operated on the island of La Palma jointly by Denmark, Finland, Iceland, Norway, and Sweden, in the Spanish Observatorio del Roque de los Muchachos of the Instituto de Astrofísica de Canarias; the 1.82 m Copernico Telescope of INAF-Asiago Observatory; the Gran Telescopio Canarias (GTC), installed in the Spanish Observatorio del Roque de los Muchachos of the Instituto de Astrofísica de Canarias, in the Island of La Palma; the Tillinghast Telescope of the Fred Lawrence Whipple Observatory; the Iowa Robotic Telescope that is located at the Winer Observatory (Arizona) and is scheduled and operated remotely from the University of Iowa; the Catalina Real Time Survey (CRTS) Catalina Sky Survey (CSS) 0.7 m Schmidt Telescope; and the Liverpool Telescope operated on the island of La Palma by Liverpool John Moores University at the Spanish Observatorio del Roque de los Muchachos of the Instituto de Astrofisica de Canarias with financial support from the UK Science and Technology Facilities Council. KAIT and its ongoing operation were made possible by donations from Sun Microsystems, Inc., the Hewlett-Packard Company, AutoScope Corporation, Lick Observatory, the NSF, the University of California, the Sylvia & Jim Katzman Foundation, and the TABASGO Foundation. Research at Lick Observatory is partially supported by a generous gift from Google.

This work made use of the NASA/IPAC Extragalactic Database (NED), which is operated by the Jet Propulsion Laboratory, California Institute of Technology, under contract with NASA. We also used NASA's Astrophysics Data System. This publication made also use of data products from the Two Micron All Sky Survey, which is a joint project of the University of Massachusetts and the Infrared Processing and Analysis Center/California Institute of Technology, funded by NASA and the NSF.

REFERENCES

Aretzaga I., Benetti S., Terlevich R. J., Fabian A. C., Cappellaro E., Turatto M., della Valle M., 1999, MNRAS, 309, 343
Arnett W. D., Meakin C., 2011, ApJ, 741, 33
Benetti S. et al., 2016, MNRAS, 456, 3296
Bilinski C., Smith N., Li W., Williams G. G., Zheng W., Filippenko A. V., 2015, MNRAS, 450, 246
Blagorodnova N. et al., 2017, ApJ, 834, 107
Bose S. et al., 2017, Astron. Telegram, 9937
Branch D., Falk S. W., Uomoto A. K., Wills B. J., McCall M. L., Rybski P., 1981, ApJ, 244, 780
Brown J. S. et al., 2016, Astron. Telegram, 9445
Cappellaro E., 2014 SNOoPy: a Package for SN Photometry (Available at http://sngroup.oapd.inaf.it/snoopy.html)
Castor J., Abbott D., Klein R., 1975, ApJ, 195, 157
Chambers K. C. et al., 2016, preprint (arXiv:1612.05560)
Chandra P., Chevalier R. A., Chugai N., Fransson C., Irwin C. M., Soderberg A. M., Chakraborti S., Immler S., 2012, ApJ, 755, 110
Chandra P., Chevalier R. A., Chugai N., Fransson C., Soderberg A. M., 2015, ApJ, 810, 32
Chatzopoulos E., Wheeler J. C., 2012, ApJ, 760, 154
Chevalier R. A., 2012, ApJ, 752, L2
Chevalier R. A., Fransson C., 1994, ApJ, 420, 268
Chevalier R. A., Irwin C. M., 2011, ApJ, 729, L6

Chonis T. S., Gaskell C. M., 2008, AJ, 135, 264
Chugai N. N., 1991, MNRAS, 250, 513
Chugai N. N. et al., 2004, MNRAS, 352, 1213
Corsi A. et al., 2014, ApJ, 782, 42
Courtois H. M., Tully R. B., 2015, MNRAS, 447, 1531
de Mink S., Langer N., Izzard R. G., Sana H., de Koter A., 2013, ApJ, 764, 166
de Mink S., Sana H., Langer N., Izzard R. G., Schneider F. R. N., 2014, ApJ, 782, 7
Dessart L., Hillier D. J., Gezari S., Basa S., Matheson T., 2009, MNRAS, 394, 21
Dessart L., Hillier D. J., Audit E., Livne E., Waldman R., 2016, MNRAS, 458, 2094
Djorgovski S. G. et al., 2012, in Mihara T., Serino M., eds, The Catalina Real-Time Transient Survey (CRTS). RIKEN, Tokyo, p. 263
Drake A. et al., 2009, ApJ, 696, 870
Dwarkadas V. V., Owocki S. P., 2002, ApJ, 581, 1337
Elias-Rosa N. et al., 2016, MNRAS, 463, 3894
Elias-Rosa N. et al., 2017, MNRAS, in press
Fassia A. et al., 2000, MNRAS, 318, 1093
Fassia A. et al., 2001, MNRAS, 325, 907
Filippenko A. V., 1982, PASP, 94, 715
Filippenko A. V., 1997, ARA&A, 35, 309
Filippenko A. V., Li W., Treffers R. R., Modjaz M., 2001, in Chen W.-P., Lemme C., Paczyński B. eds, ASP Conf. Ser., Vol. 246, Small-Telescope Astronomy on Global Scales. Astron. Soc. Pac., San Francisco, p. 121
Foley R. J, Smith N., Ganeshalingam M., Li W., Chornock R., Filippenko A. V., 2007, ApJ, 657, L105
Foley R. J, Berger E., Fox O., Levesque E. M., Challis P. J., Ivans I. I., Rhoads J. E., Soderberg A. M., 2011, ApJ, 732, 32
Fransson C. et al., 2005, ApJ, 622, 991
Fraser M. et al., 2013a, MNRAS, 433, 1312
Fraser M. et al., 2013b, ApJ, 779, L8
Fraser M. et al., 2015, MNRAS, 453, 3886
Fraser M. et al., 2017, Astron. Telegram, 9938
Gal-Yam A., Leonard D. C., 2009, Nature, 458, 865
Gal-Yam A. et al., 2007, ApJ, 656, 372
Garcia-Benito R. et al., 2015, A&A, 576, 135
Ginzburg S., Balberg S., 2012, AJ, 757, 178
Goranskij V. P., Barsukova E. A., Valeev A. F., Tsvetkov D. Yu., Volkov I. M., Metlov V. G., Zharova A. V., 2016, Astrophys. Bull., 71, 422
Graham M. L. et al., 2014, ApJ, 787, 163
Graham M. L. et al., 2017, MNRAS, 469, 1559
Heger A., Fryer C. L., Woosley S. E., Langer N., Hartmann D. H., 2003, ApJ, 591, 288
Hosseinzadeh G. et al., 2017, ApJ, 836, 158
Huber M. et al., 2015, Astron. Telegram, 7153
Humphreys R. M., Davidson K., 1994, PASP, 106, 1025
Humphreys R. M., Davidson K., Jones T. J., Pogge R. W., Grammer S. H., Prieto J. L., Pritchard T. A., 2012, ApJ, 760, 93
Justham S., Podsiadlowski P., Vink J. S., 2014, ApJ, 796, 121
Kashi A., 2010, MNRAS, 405, 1924
Kashi A., Soker N., 2010, ApJ, 723, 602
Kashi A., Soker N., Moskovitz N., 2013, MNRAS, 436, 2484
Kiewe M. et al., 2012, ApJ, 744, 10
Kilpatrick R. J. et al., 2017, MNRAS, preprint (arXiv:1706.09962)
Kochanek C. S., Adams S. M., Belczynski K., 2014, MNRAS, 443, 1319
Laher R. R. et al., 2014, PASP, 126, L674
Lamers H. J. G. L. M., Nugis T., 2002, A&A, 395, L1
Langer N., 2012, ARA&A, 50, 107
Langer N., García-Segura G., Mac Low M.-M., 1999, ApJ, 520, L49
Law N. M. et al., 2009, PASP, 121, 1395
Leaman J., Li W., Chornock R., Filippenko A. V., 2011, MNRAS, 412, 1419
Levesque E. M., Stringfellow G. S., Ginsburg A. G., Bally J., Keeney B. A., 2014, AJ, 147, L23
Margutti R. et al., 2014, ApJ, 780, 21
Martin J. C., Hambsch F.-J., Margutti R., Tan T. G., Curtis I., Soderberg A., 2015, AJ, 149, 9
Mattila S. et al., 2016, Astron. Telegram, 8992
Mauerhan J. C. et al., 2013a, MNRAS, 430, 1801
Mauerhan J. C. et al., 2013b, MNRAS, 431, 2599
Mauerhan J. C. et al., 2014, MNRAS, 442, 1166
Mauerhan J. C., Van Dyk S. D., Johansson J., Fox O. D., Filippenko A. V., Graham M. L., 2017, MNRAS, preprint (arXiv:1702.00430)
Maund J. R. et al., 2006, MNRAS, 369, 390
Moriya T. J., 2015, ApJ, 803, L26
Moriya T. J., Langer N., 2014, A&A, 573, 18
Moriya T., Tominaga N., Tanaka M., Nomoto K., Sauer D. N., Mazzali P. A., Maeda K., Suzuki T., 2010, ApJ, 719, 1445
Moriya T., Tominaga N., Blinnikov S. I., Baklanov P. V., Sorokina E. I., 2011, MNRAS, 415, 199
Nomoto L., Tominaga N., Umeda H., Kobayashi C., Maeda K., 2006, Nucl. Phys. A, 777, 424
Nyholm A. et al., 2017, A&A, 605, A6
Ofek E. O. et al., 2016, ApJ, 824, 6
Ofek E. O. et al., 2012, PASP, 124, 854
Ofek E. O. et al., 2013a, Nature, 494, 65
Ofek E. O. et al., 2013b, ApJ, 768, 47
Ofek E. O. et al., 2014, ApJ, 789, 104
Owocki S. P., Puls J., 1999, ApJ, 510, 355
Pastorello A. et al., 2002, MNRAS, 333, 27
Pastorello A. et al., 2007, Nature, 447, 829
Pastorello A. et al., 2008, MNRAS, 389, 113
Pastorello A. et al., 2010, MNRAS, 408, 181
Pastorello A. et al., 2012, A&A, 537, 141
Pastorello A. et al., 2013a, ApJ, 767, 1
Pastorello A. et al., 2013b, Astron. Telegram, 5358
Pastorello A. et al., 2016, MNRAS, 456, 853
Pejcha O., Thompson T. A., 2015, ApJ, 801, 90
Portegies Zwart S. F., van den Heuvel E. P. J., 2016, MNRAS, 456, 3401
Prieto J. L., Brimacombe J., Drake A. J., Howerton S., 2013, ApJ, 763, L27
Sana H. et al., 2012, Science, 337, 444
Schlafly E. F., Finkbeiner D. P., 2011, ApJ, 737, 103
Schlegel, 1990, MNRAS, 244, 269
Shappee B. J. et al., 2014, ApJ, 788, 48
Shiode J. H., Quataert E., 2014, ApJ, 780, 96
Skrutskie M. F. et al., 2006, AJ, 131, 1163
Smith N., 2013, MNRAS, 434, 102
Smith N., 2014, ARA&A, 52, 487
Smith N., Frew D. J., 2011, MNRAS, 415, 2009
Smith N. et al., 2010, AJ, 139, 1451
Smith N., Mauerhan J. C., Kasliwal M. M., Burgasser A. J., 2013, MNRAS, 434, 2721
Smith N., Mauerhan J. C., Prieto J. L., 2014, MNRAS, 438, 1191
Smith N. et al., 2016a, MNRAS, 458, 950
Smith N., Andrews J. E., Mauerhan J. C., 2016b, MNRAS, 463, 2904
Smith N. et al., 2017, MNRAS, 466, 3021
Soker N., 2012, New Astron., 18, 18
Soker N., Kashi A., 2013, ApJ, 764, L6
Soker N., Kashi A., 2016, MNRAS, 462, 217
Strotjohann N. L. et al., 2015, ApJ, 811, 117
Sukhbold T., Ertl T., Woosley S. E., Brown J. M., Janka H.-T., 2014, ApJ, 821, 38
Svirski G., Nakar E., Sari R., 2012, ApJ, 759, 108
Taddia F. et al., 2013, A&A, 555, 10
Tartaglia L. et al., 2016, MNRAS, 459, 1039
Terreran G. et al., 2016a, Astron. Telegram, 9111
Terreran G. et al., 2016b, MNRAS, 462, 137
Thöne C. C. et al., 2017, A&A, 599, 129
Tonry J. L., 2011, PASP, 123, 899
Tsebrenko D., Soker N., 2013, ApJ, 777, L35
Van Dyk S. D., Peng C. Y., King J. Y., Filippenko A. V., Treffers R. R., Li W., Richmond M. W., 2000, PASP, 112, 1532
Wagner R. M. et al., 2004, PASP, 116, 326

Walton N. et al., 2015, Astron. Telegram, 7308
Weiler K. W., Sramek R. A., Panagia N., van del Hulst J. M., Salvati M., 1986, ApJ, 301, 790
Woosley S. E., Blinnikov S., Heger A., 2007, Nature, 450, 390
Yaron O., Gal-Yam A., 2012, PASP, 124, 668
Zampieri L., Shapiro S. L., Colpi M., 1998, ApJ, 502, L149

APPENDIX A: PHOTOMETRIC DATA FOR SN 2016BDU

Johnson–Bessell *B* and *V*, Sloan *u*, *g*, *r*, *i*, and *z*, and NIR *J*, *H*, and *K* magnitudes of SN 2016bdu are reported in Tables A1, A2, and A3, respectively.

Table A1. Optical photometry (Johnson–Bessell, Vega mag) of SN 2016bdu.

Date	JD	*B*	*V*	Instrument
1998-04-23	245 0926.89	–	>19.84	1
1998-06-19	245 0984.43	–	>23.78	2
2001-07-01	245 2091.69	–	>20.94	1
2002-03-02	245 2336.05	–	>20.40	1
2002-05-21	245 2395.72	–	>21.21	1
2003-02-19	245 2690.05	–	>20.45	1
2016-02-18	245 7436.91	–	>17.64	3
2016-02-19	245 7438.14	–	>18.37	3
2016-02-20	245 7438.91	–	>17.27	3
2016-02-22	245 7440.98	–	>17.15	3
2016-02-24	245 7443.17	–	>16.01	3
2016-02-25	245 7443.98	–	>17.44	3
2016-02-27	245 7446.11	–	>17.79	3
2016-02-29	245 7447.97	–	>18.12	3
2016-03-02	245 7450.01	–	>18.21	3
2016-03-04	245 7451.99	–	>18.42	3
2016-03-07	245 7454.87	–	>18.39	3
2016-03-11	245 7458.93	–	>18.51	3
2016-03-14	245 7461.92	–	>17.75	3
2016-03-16	245 7463.86	–	>17.35	3
2016-03-19	245 7466.84	–	>17.29	3
2016-03-22	245 7469.99	–	>16.93	3
2016-03-25	245 7472.95	–	>17.04	3
2016-03-28	245 7475.85	–	>18.06	3
2016-03-31	245 7478.89	–	>18.38	3
2016-04-03	245 7481.97	–	>18.31	3
2016-04-10	245 7488.85	–	>18.24	3
2016-04-12	245 7490.97	–	>18.42	3
2016-04-16	245 7494.77	–	>17.35	3
2016-04-20	245 7498.96	–	>16.83	3
2016-04-23	245 7501.89	–	>17.20	3
2016-04-27	245 7505.91	–	>18.12	3
2016-04-28	245 7506.83	–	>18.40	3
2016-05-02	245 7510.89	–	>18.47	3
2016-05-05	245 7513.89	–	>18.72	3
2016-05-05	245 7513.90	–	>19.32	4
2016-05-13	245 7521.78	–	>17.68	3
2016-05-15	245 7523.93	–	>17.77	3
2016-05-20	245 7528.74	–	>17.33	3
2016-05-21	245 7529.89	–	>17.14	3
2016-05-29	245 7537.89	–	16.509 (0.084)	3
2016-05-30	245 7538.80	–	16.486 (0.075)	3
2016-06-02	245 7541.81	16.529 (0.019)	16.478 (0.036)	5
2016-06-03	245 7542.85	–	16.343 (0.033)	4
2016-06-03	245 7542.88	–	16.556 (0.132)	3
2016-06-04	245 7543.88	–	16.426 (0.084)	3
2016-06-07	245 7546.85	–	16.500 (0.024)	4
2016-06-09	245 7548.87	–	16.606 (0.084)	3
2016-06-12	245 7551.79	–	16.909 (0.143)	3
2016-06-13	245 7552.80	16.900 (0.049)	16.774 (0.065)	6
2016-06-14	245 7553.56	16.961 (0.036)	16.807 (0.022)	7
2016-06-14	245 7553.80	16.994 (0.065)	16.791 (0.074)	6
2016-06-16	245 7555.85	17.119 (0.070)	16.858 (0.107)	6
2016-06-17	245 7556.83	–	16.805 (0.141)	6

Table A1 – *continued*

Date	JD	*B*	*V*	Instrument
2016-06-17	245 7557.41	17.201 (0.209)	–	8
2016-06-20	245 7559.82	–	17.046 (0.271)	3
2016-06-22	245 7561.92	17.444 (0.030)	17.156 (0.041)	8
2016-06-23	245 7562.79	–	17.45 (0.16)	3
2016-06-29	245 7568.78	–	>18.06	3
2016-07-03	245 7572.73	–	17.959 (0.106)	5
2016-07-04	245 7573.75	–	17.974 (0.099)	5
2016-07-04	245 7574.50	18.619 (0.024)	18.054 (0.032)	7
2016-07-13	245 7582.78	–	18.23 (0.15)	4
2016-07-15	245 7584.67	19.084 (0.134)	–	5
2016-07-15	245 7585.48	19.101 (0.032)	18.348 (0.030)	7
2016-07-21	245 7591.40	19.258 (0.022)	18.464 (0.020)	7
2016-07-28	245 7598.42	19.415 (0.027)	18.578 (0.029)	7
2016-08-04	245 7605.41	20.075 (0.036)	19.067 (0.023)	7
2016-08-06	245 7606.79	–	>19.19	4
2016-08-12	245 7613.44	20.781 (0.078)	19.930 (0.050)	9
2016-08-18	245 7619.39	21.115 (0.088)	20.205 (0.030)	7
2016-08-23	245 7624.31	–	20.341 (0.143)	8
2016-08-27	245 7628.39	21.316 (0.066)	20.419 (0.057)	7
2016-12-23	245 7746.16	–	>19.88	5
2016-12-29	245 7751.71	–	21.952 (0.101)	7
2016-12-31	245 7746.16	–	>19.73	5
2017-01-05	245 7758.78	22.836 (0.299)	–	7
2017-01-24	245 7777.53	>22.87	22.227 (0.581)	8
2017-02-19	245 7803.73	23.605 (0.396)	22.417 (0.241)	7
2017-03-26	245 7838.61	–	23.012 (0.129)	7

Notes. 1 = NEAT images; 2 = 2.54 m INT + WFC; 3 = ASAS-SN telescopes; 4 = ATLAS telescopes; 5 = Meade 10" LX-200 Telescope + Apogee Alte F-47 CCD; 6 = 0.51 m Iowa Robotic Telescope + Apogee Alta F-47 CCD; 7 = 2.56 m NOT + ALFOSC; 8 = 1.82 m Copernico Telescope + AFOSC; 9 = 3.54 m TNG + LRS.

Table A2. Optical photometry (Sloan AB mag) of SN 2016bdu.

Date	JD	*u*	*g*	*r*	*i*	*z*	Instrument
1998-06-19	245 0984.44	–	–	–	>23.65	–	1
1999-02-10	245 1219.72	–	–	23.463 (0.391)	–	–	1
2003-04-01	245 2730.79	–	–	>20.00[a]	–	–	2
2004-03-19	245 3083.88	–	–	>20.74[a]	–	–	2
2004-04-19	245 3114.80	–	–	>20.79[b]	–	–	2
2004-04-28	245 3123.78	–	–	>19.93[b]	–	–	2
2004-05-20	245 3145.89	–	–	>20.69[b]	–	–	2
2005-03-08	245 3437.42	–	–	>20.63	–	–	2
2005-03-14	245 3443.43	–	–	20.60 (0.37)	–	–	2
2005-03-31	245 3460.39	–	–	>20.64	–	–	2
2005-04-11	245 3471.32	–	–	>20.62	–	–	2
2005-04-19	245 3479.20	–	–	>20.39	–	–	2
2005-05-01	245 3491.22	–	–	>20.72	–	–	2
2005-05-14	245 3504.27	–	–	20.65 (0.62)	–	–	2
2005-06-06	245 3527.29	–	–	>20.33	–	–	2
2006-02-04	245 3771.52	–	–	>20.69	–	–	2
2006-03-03	245 3798.47	–	–	>20.39	–	–	2
2006-03-29	245 3824.57	–	–	>20.60	–	–	2
2006-04-08	245 3834.11	–	–	>20.27	–	–	2
2006-04-27	245 3852.99	–	–	>20.26	–	–	2
2006-05-06	245 3862.25	–	–	>20.49	–	–	2
2006-06-01	245 3888.17	–	–	>20.49	–	–	2
2006-06-16	245 3902.82	–	–	>18.75	–	–	2
2007-02-10	245 4141.96	–	–	>20.11	–	–	2
2007-02-25	245 4156.80	–	–	>20.66	–	–	2
2007-03-10	245 4169.81	–	–	>21.10	–	–	2
2007-03-17	245 4176.91	–	–	>20.45	–	–	2
2007-04-19	245 4209.83	–	–	>20.69	–	–	2
2007-04-26	245 4216.66	–	–	>20.42	–	–	2

Table A2 – *continued*

Date	JD	*u*	*g*	*r*	*i*	*z*	Instrument
2007-05-15	245 4235.72	–	–	>20.58	–	–	2
2007-05-24	245 4244.74	–	–	>20.28	–	–	2
2007-06-05	245 4256.75	–	–	>20.63	–	–	2
2007-06-12	245 4263.74	–	–	>20.31	–	–	2
2007-06-21	245 4272.69	–	–	20.44 (0.67)	–	–	2
2008-01-17	245 4483.01	–	–	>20.51	–	–	2
2008-02-12	245 4508.83	–	–	>20.56	–	–	2
2008-02-18	245 4514.87	–	–	>20.38	–	–	2
2008-03-02	245 4527.86	–	–	>20.48	–	–	2
2008-03-08	245 4533.85	–	–	>20.59	–	–	2
2008-03-24	245 4549.92	–	–	>20.46	–	–	2
2008-04-01	245 4557.86	–	–	20.32 (0.60)	–	–	2
2008-04-08	245 4564.83	–	–	>20.56	–	–	2
2008-04-14	245 4570.69	–	–	>20.42	–	–	2
2008-05-03	245 4589.75	–	–	>20.52	–	–	2
2008-05-13	245 4599.64	–	–	20.22 (0.68)	–	–	2
2008-06-12	245 4629.74	–	–	>20.53	–	–	2
2008-12-07	245 4807.98	–	–	>20.74	–	–	2
2009-02-26	245 4888.88	–	–	>20.63	–	–	2
2009-03-17	245 4907.96	–	–	>20.55	–	–	2
2009-03-24	245 4914.81	–	–	>20.68	–	–	2
2009-04-02	245 4923.71	–	–	>20.53	–	–	2
2009-04-21	245 4942.74	–	–	20.41 (0.58)	–	–	2
2009-05-13	245 4964.27	–	–	>20.90	–	–	3
2009-05-15	245 4966.27	–	–	21.15 (0.27)	–	–	3
2009-05-17	245 4968.79	–	–	>20.59	–	–	2
2009-05-19	245 4970.28	–	–	>19.48	–	–	3
2009-05-30	245 4981.70	–	–	>20.40	–	–	2
2009-06-30	245 5012.20	–	–	21.26 (0.35)	–	–	3
2009-07-28	245 5040.66	–	–	>20.05	–	–	2
2010-03-05	245 5260.98	–	–	>20.45	–	–	2
2010-03-16	245 5271.81	–	–	20.56 (0.63)	–	–	2
2010-03-25	245 5280.76	–	–	>20.56	–	–	2
2010-04-12	245 5298.88	–	–	>20.59	–	–	2
2010-05-05	245 5321.84	–	–	>20.40	–	–	2
2010-05-14	245 5330.78	–	–	>19.99	–	–	2
2010-05-15	245 5331.77	–	–	>20.28	–	–	2
2010-05-17	245 5333.81	–	–	>20.71	–	–	2
2010-05-25	245 5341.79	–	–	>20.36	–	–	2
2010-06-02	245 5349.18	–	–	>21.08	–	–	3
2010-06-08	245 5355.68	–	–	>20.06	–	–	2
2010-06-12	245 5359.71	–	–	>20.33	–	–	2
2011-02-23	245 5615.97	–	–	>20.58	–	–	2
2011-03-08	245 5628.85	–	–	>20.30	–	–	2
2011-03-14	245 5634.85	–	–	>20.65	–	–	2
2011-03-27	245 5647.77	–	–	>20.65	–	–	2
2011-04-08	245 5659.80	–	–	>20.85	–	–	2
2011-04-28	245 5679.87	–	–	>20.74	–	–	2
2011-06-10	245 5722.74	–	–	>20.68	–	–	2
2012-01-29	245 5955.91	–	–	20.60 (0.50)	–	–	2
2012-02-24	245 5981.86	–	–	20.47 (0.42)	–	–	2
2012-03-15	245 6001.96	–	–	20.89 (0.44)	–	–	2
2012-03-22	245 6008.90	–	–	20.20 (0.25)	–	–	2
2012-03-29	245 6015.84	–	–	20.21 (0.40)	–	–	2
2012-04-16	245 6033.86	–	21.636 (0.173)	20.911 (0.084)	–	–	4
2012-04-20	245 6037.72	–	–	>20.59	–	–	2
2012-05-18	245 6065.77	–	–	>20.62	–	–	2
2012-06-10	245 6088.68	–	–	>20.48	–	–	2
2012-06-18	245 6096.72	–	–	>20.55	–	–	2
2013-01-22	245 6314.86	–	–	>20.80	–	–	2
2013-03-02	245 6353.98	–	–	>20.37	–	–	2
2013-03-17	245 6368.87	–	–	>20.92	–	–	2
2013-04-12	245 6394.84	–	–	>18.92	–	–	2
2013-04-13	245 6395.85	–	–	>20.24	–	–	2

Table A2 – *continued*

Date	JD	*u*	*g*	*r*	*i*	*z*	Instrument
2013-04-21	245 6403.72	–	–	>20.33	–	–	2
2013-05-04	245 6416.70	–	–	>20.41	–	–	2
2013-06-05	245 6448.77	–	–	>20.66	–	–	2
2013-06-18	245 6461.75	–	–	>20.59	–	–	2
2014-01-02	245 6659.96	–	–	>20.60	–	–	2
2014-02-09	245 6698.14	–	>21.64	–	–	>20.32	4
2014-02-21	245 6710.13	–	–	>21.68	–	>20.75	4
2014-03-09	245 6725.88	–	–	>20.67	–	–	2
2014-03-18	245 6735.04	–	–	–	21.442 (0.288)	–	4
2014-03-26	245 6742.79	–	–	>20.70	–	–	2
2014-03-27	245 6743.91	–	21.630 (0.174)	–	–	–	4
2014-04-01	245 6748.75	–	–	>20.88	–	–	2
2014-04-09	245 6756.84	–	–	>20.62	–	–	2
2014-04-25	245 6772.84	–	–	>20.76	–	–	2
2014-05-03	245 6780.81	–	–	>20.33	–	–	2
2014-05-26	245 6803.78	–	–	>20.77	–	–	2
2014-06-06	245 6814.77	–	–	>20.29	–	–	2
2014-06-21	245 6829.77	–	–	>20.28	–	–	2
2015-01-18	245 7040.85	–	–	>20.57	–	–	2
2015-01-25	245 7047.83	–	–	>20.49	–	–	2
2015-02-09	245 7062.94	–	–	>20.58	–	–	2
2015-02-10	245 7064.17	–	–	–	–	>19.13	4
2015-02-11	245 7065.17	–	–	–	–	>20.22	4
2015-02-19	245 7072.96	–	–	>20.65	–	–	2
2015-03-03	245 7085.11	–	–	–	>21.05	–	4
2015-03-10	245 7092.01	–	–	>20.57	–	–	2
2015-03-17	245 7098.88	–	–	>20.60	–	–	2
2015-03-24	245 7105.78	–	–	>20.62	–	–	2
2015-04-10	245 7122.76	–	–	>20.65	–	–	2
2015-04-16	245 7128.89	–	–	>20.55	–	–	2
2015-04-23	245 7135.79	–	–	20.70 (0.42)	–	–	2
2015-05-19	245 7161.73	–	–	20.10 (0.40)	–	–	2
2015-05-25	245 7167.66	–	–	20.59 (0.33)	–	–	2
2015-06-15	245 7188.67	–	–	>20.90	–	–	2
2015-06-29	245 7202.81	–	–	–	>21.70	–	4
2015-06-30	245 7203.79	–	–	–	>21.53	–	4
2015-12-25	245 7382.12	–	–	–	>20.31	–	4
2016-01-18	245 7406.03	–	–	>20.68	–	–	2
2016-01-30	245 7418.01	–	–	>20.63	–	–	2
2016-01-31	245 7419.05	–	–	21.672 (0.243)	–	–	4
2016-02-06	245 7424.99	–	–	>20.39	–	–	2
2016-02-13	245 7432.00	–	–	20.50 (0.35)	–	–	2
2016-02-28	245 7446.97	–	–	20.77 (0.72)	–	–	2
2016-02-28	245 7447.13	–	–	20.729 (0.170)	–	–	4
2016-03-04	245 7452.14	–	–	–	–	20.307 (0.245)	4
2016-03-12	245 7459.95	–	–	20.83 (0.55)	–	–	2
2016-03-18	245 7465.93	–	–	20.621 (0.132)	–	–	4
2016-03-18	245 7465.94	–	–	20.64 (0.41)	–	–	2
2016-03-18	245 7465.94	–	–	20.656 (0.139)	–	–	4
2016-03-28	245 7475.90	–	–	19.945 (0.053)	–	–	4
2016-03-31	245 7478.77	–	–	19.78 (0.40)	–	–	2
2016-04-06	245 7484.76	–	–	19.85 (0.33)	–	–	2
2016-04-27	245 7505.72	–	–	19.14 (0.21)	–	–	2
2016-05-05	245 7513.90	–	>19.43	–	–	–	5
2016-05-08	245 7516.84	–	–	19.44 (0.25)	–	–	2
2016-05-20	245 7528.86	–	–	>18.75	–	–	5
2016-05-24	245 7532.87	–	–	16.909 (0.071)	–	–	5
2016-05-24	245 7532.91	–	–	–	17.167 (0.022)	–	4
2016-05-28	245 7536.86	–	–	16.438 (0.080)	–	–	5
2016-06-02	245 7541.80	–	–	16.385 (0.197)	–	–	2
2016-06-02	245 7541.80	–	–	16.434 (0.030)	16.498 (0.035)	–	6
2016-06-02	245 7542.48	–	–	16.355 (0.165)	–	–	7
2016-06-03	245 7542.85	–	16.412 (0.049)	–	–	–	5
2016-06-07	245 7546.85	–	16.569 (0.043)	–	–	–	5

Table A2 – *continued*

Date	JD	*u*	*g*	*r*	*i*	*z*	Instrument
2016-06-12	245 7552.42	17.048 (0.015)	16.838 (0.014)	16.710 (0.017)	16.836 (0.017)	–	8
2016-06-13	245 7552.81	–	16.820 (0.026)	16.756 (0.061)	16.814 (0.050)	–	9
2016-06-14	245 7553.56	17.123 (0.033)	16.787 (0.020)	16.751 (0.017)	16.830 (0.021)	16.960 (0.014)	7
2016-06-14	245 7553.80	–	16.826 (0.037)	16.779 (0.074)	16.853 (0.064)	–	9
2016-06-14	245 7554.49	17.180 (0.025)	16.847 (0.024)	16.769 (0.019)	16.888 (0.015)	–	8
2016-06-16	245 7555.83	–	16.936 (0.073)	16.867 (0.079)	16.912 (0.052)	–	9
2016-06-17	245 7557.41	17.553 (0.067)	16.954 (0.036)	16.957 (0.046)	17.036 (0.037)	17.251 (0.036)	10
2016-06-18	245 7557.81	–	–	>17.06	–	–	5
2016-06-18	245 7558.48	17.609 (0.019)	17.037 (0.022)	17.003 (0.026)	17.066 (0.025)	–	8
2016-06-21	245 7561.44	18.172 (0.030)	17.382 (0.014)	17.171 (0.020)	17.296 (0.031)	–	8
2016-06-22	245 7561.82	–	–	17.200 (0.039)	–	–	5
2016-06-22	245 7562.43	18.228 (0.050)	17.431 (0.065)	17.234 (0.036)	17.368 (0.031)	17.426 (0.028)	10
2016-06-26	245 7565.82	–	–	17.451 (0.045)	–	–	5
2016-07-01	245 7571.50	–	–	17.688 (0.193)	–	–	7
2016-07-03	245 7572.69	–	–	17.825 (0.187)	–	–	6
2016-07-04	245 7573.51	19.623 (0.033)	18.372 (0.033)	17.877 (0.024)	17.948 (0.021)	17.912 (0.020)	7
2016-07-04	245 7573.67	–	–	17.912 (0.197)	–	–	6
2016-07-13	245 7582.78	–	18.481 (0.152)	–	–	–	5
2016-07-14	245 7583.68	–	–	18.078 (0.201)	–	–	6
2016-07-15	245 7585.49	20.259 (0.118)	18.674 (0.038)	18.105 (0.021)	18.047 (0.018)	18.074 (0.036)	7
2016-07-17	245 7587.41	–	–	18.102 (0.084)	–	–	11
2016-07-21	245 7591.41	–	18.793 (0.027)	18.203 (0.022)	18.153 (0.031)	18.087 (0.035)	7
2016-07-28	245 7598.43	–	18.991 (0.028)	18.291 (0.014)	18.275 (0.014)	18.177 (0.029)	7
2016-07-29	245 7599.43	–	–	18.317 (0.349)	–	–	7[c]
2016-07-30	245 7599.77	–	–	18.333 (0.198)	–	–	5
2016-08-04	245 7605.43	21.398 (0.127)	19.600 (0.020)	18.470 (0.019)	18.399 (0.018)	18.446 (0.037)	7
2016-08-06	245 7606.79	–	>19.29	–	–	–	5
2016-08-10	245 7611.42	–	20.233 (0.058)	19.176 (0.024)	19.202 (0.026)	19.106 (0.041)	7
2016-08-18	245 7619.40	–	20.601 (0.055)	19.529 (0.024)	19.578 (0.029)	19.488 (0.036)	7
2016-08-19	245 7620.37	–	–	19.599 (0.085)	–	–	11
2016-08-22	245 7623.34	–	–	19.650 (0.040)	19.771 (0.062)	19.532 (0.079)	10
2016-08-23	245 7624.31	>20.91	20.682 (0.244)	–	–	–	10
2016-08-27	245 7628.31	–	–	19.778 (0.065)	19.870 (0.088)	19.652 (0.064)	10
2016-08-27	245 7628.39	–	20.772 (0.121)	–	–	–	7
2016-12-23	245 7746.16	–	>20.91	–	–	–	5
2016-12-29	245 7751.74	–	22.693 (0.081)	20.898 (0.040)	21.872 (0.072)	21.639 (0.144)	7
2016-12-31	245 7754.16	–	>20.76	–	–	–	5
2017-01-05	245 7758.77	>22.36	–	–	–	–	7
2017-01-20	245 7773.61	–	–	20.947 (0.299)	–	–	11
2017-01-24	245 7777.53	–	–	–	22.106 (0.275)	–	10
2017-01-25	245 7778.65	–	22.880 (0.296)	20.969 (0.128)	22.130 (0.324)	21.881 (0.460)	10
2017-02-19	245 7803.74	–	23.254 (0.263)	21.245 (0.032)	22.341 (0.082)	>21.92	7
2017-03-26	245 7838.63	–	23.335 (0.097)	21.437 (0.042)	22.534 (0.086)	22.208 (0.182)	7

Notes. 1 = 2.54 m INT + WFC; 2 = CRTS Telescope; 3 = PTF Telescope (*R* filter, Sloan *r* calibrated); 4 = PS1; 5 = ATLAS Telescopes ('open' filter, Sloan *r* calibrated); 6 = Meade 10" LX-200 Telescope + Apogee Alte F-47 CCD; 7 = 2.56 m NOT + ALFOSC; 8 = 2.0 m LT + IO:O; 9 = 0.51 m Iowa Robotic Telescope + Apogee Alta F-47 CCD; 10 = 1.82 m Copernico Telescope + AFOSC; 11 = 10.4 m GTC + OSIRIS.
[a] *Y* filter, Sloan *r* calibrated; [b] *R* filter, Sloan *r* calibrated; [c] unfiltered observation, Sloan *r* calibrated.

Table A3. Near-infrared photometry of SN 2016bdu.

Date	JD	*J*	*H*	*K*
2016-06-11	245 7551.48	16.41 (0.18)	16.32 (0.25)	16.05 (0.23)
2016-06-23	245 7562.50	16.73 (0.19)	16.63 (0.24)	16.35 (0.23)
2016-07-14	245 7584.44	17.18 (0.21)	17.12 (0.21)	16.82 (0.16)
2016-07-27	245 7597.40	17.34 (0.20)	17.21 (0.19)	16.94 (0.16)
2016-08-11	245 7612.43	18.39 (0.16)	18.15 (0.30)	17.64 (0.25)
2016-08-22	245 7623.38	18.80 (0.22)	18.51 (0.39)	17.92 (0.30)
2017-01-10	245 7763.68	20.60 (0.24)	20.67 (0.38)	20.31 (0.24)
2017-02-07	245 7791.63	21.21 (0.32)	20.95 (0.46)	20.42 (0.39)
2017-03-24	245 7837.45	21.76 (0.25)	21.18 (0.45)	20.86 (0.47)

Note. Observations obtained using the 2.56 m NOT + NOTCam.

APPENDIX B: PHOTOMETRIC DATA FOR SN 2005GL

We remeasured the unfiltered KAIT images of SN 2005gl previously published by Gal-Yam et al. (2007), and collected new data from amateur astronomers. These unfiltered photometric data were calibrated to the Johnson–Cousins *R* band. The *R*-band calibration, in fact, provided more accurate results because the quantum efficiency curves of the CCDs used in these observations typically peaked at $\lambda \geq 6000$ Å. For the calibration, we used the *R*-band magnitudes of comparison stars from Gal-Yam et al. (2007). There is a significant offset from the magnitudes provided by Gal-Yam et al. (2007). This disagreement is likely due to the fact that we did not use Stars 4 and 7 of Gal-Yam et al. (2007) for our calibration. These two stars were rejected because the $V - R$ colours reported in table 2 of Gal-Yam et al. (2007) are extremely blue (−0.26 mag and −0.22 mag for Stars 4 and 7, respectively), in contrast with the relatively red colours reported for these two stars in the Sloan catalogue ($g - r \approx 1.2$ mag). The photometry for both data sets was obtained with the template-subtraction method.

Table B1. Photometry of SN 2005gl (unfiltered KAIT and amateur), rescaled to Johnson–Cousins *R* (Vega mag).

Date	Average JD	*R*	Instrument
stack 1998-10-20 to 1999-01-12	245 1149.75	>20.90	1
stack 1999-06-29 to 2000-01-06	245 1460.42	>20.84	1
stack 2000-07-10 to 2000-01-13	245 1819.98	>21.11	1
stack 2001-07-31 to 2001-12-15	245 2179.42	>20.87	1
stack 2002-07-18 to 2003-01-08	245 2552.11	>21.13	1
stack 2003-07-15 to 2003-02-22	245 2898.56	>21.37	1
2005-07-22	245 3573.94	19.99 (0.45)	1
2005-07-28	245 3579.97	>19.73	1
2005-08-03	245 3585.94	>20.22	1
2005-08-09	245 3591.95	>20.20	1
2005-08-15	245 3597.86	>17.39	1
2005-08-20	245 3602.89	>19.89	1
2005-08-26	245 3608.87	>20.42	1
stack 2005-08-03 to 2005-09-14	245 3610.36	>20.84	1
2005-08-31	245 3613.85	>20.50	1
2005-09-09	245 3622.81	>20.62	1
2005-09-14	245 3627.80	>20.20	1
2005-10-02	245 3645.80	>16.97	1
2005-10-05	245 3648.60	18.81 (0.66)	2
2005-10-06	245 3649.60	18.22 (0.39)	2
2005-10-08	245 3651.81	>17.53	1
2005-10-12	245 3656.09	17.61 (0.15)	2
2005-10-13	245 3656.73	17.50 (0.11)	1
2005-10-13	245 3657.05	17.46 (0.12)	2
2005-10-15	245 3659.37	17.19 (0.12)	3
2005-10-16	245 3660.05	17.09 (0.11)	2
2005-10-18	245 3661.92	16.91 (0.09)	2
2005-10-20	245 3663.82	16.75 (0.13)	1
2005-10-20	245 3664.06	16.76 (0.09)	2
2005-10-25	245 3668.74	16.80 (0.13)	1
2005-10-25	245 3669.39	16.81 (0.04)	4
2005-10-27	245 3670.89	16.82 (0.10)	2
2005-10-27	245 3671.06	16.82 (0.06)	2
2005-10-27	245 3671.29	16.84 (0.09)	5
2005-10-27	245 3671.31	16.85 (0.06)	4
2005-10-31	245 3674.79	16.94 (0.07)	1
2005-11-06	245 3680.24	17.04 (0.12)	1
2005-11-07	245 3682.35	17.06 (0.06)	4
2005-11-07	245 3682.37	17.14 (0.10)	5
2005-11-15	245 3689.92	17.24 (0.14)	2
2005-11-17	245 3692.34	17.26 (0.09)	4
2005-11-20	245 3694.75	17.36 (0.14)	1
2005-11-20	245 3695.26	17.37 (0.06)	4
2005-11-20	245 3695.37	17.36 (0.05)	3
2005-11-26	245 3700.80	17.57 (0.21)	1
2005-11-30	245 3705.33	17.72 (0.19)	5
2005-12-07	245 3711.68	18.24 (0.11)	1
2005-12-18	245 3723.24	18.83 (0.26)	4
2005-12-21	245 3726.23	19.18 (0.21)	5

Table B1 – *continued*

Date	Average JD	*R*	Instrument
2005-12-25	245 3729.67	19.87 (0.35)	1
2005-12-26	245 3731.27	19.94 (0.33)	4
2006-01-06	245 3742.26	20.20 (0.45)	3
2006-01-16	245 3751.61	20.58 (0.53)	1
2006-07-08	245 3924.91	>20.40	1
2006-07-15	245 3931.98	>20.35	1

Notes. 1 = KAIT data; 2 = 0.28 m C11 reflector + SBIG ST-9E CCD camera (Obs. Y. Sano, Nayoro, Japan); 3 = 0.356 m Meade LX200 Telescope + SBIG ST-9XE CCD camera (Obs. E. Prosperi, Larciano, Italy); 4 = 0.28 m C11 reflector + SBIG ST-8XME Kaf1602E CCD camera (Obs. J. Nicolas; Vallauris, France); 5 = 0.28 m C11 reflector + SBIG ST-8XME Kaf1602E CCD camera (Obs. J.-M. Llapasset; Perpignan, France).

[1]*INAF-Osservatorio Astronomico di Padova, Vicolo dell'Osservatorio 5, I-35122 Padova, Italy*
[2]*Department of Astronomy, The Ohio State University, 140 West 18th Avenue, Columbus, OH 43210, USA*
[3]*Center for Cosmology and AstroParticle Physics (CCAPP), The Ohio State University, 191 W. Woodruff Ave., Columbus, OH 43210, USA*
[4]*School of Physics, O'Brien Centre for Science North, University College Dublin, Belfield, Dublin 4, Ireland*
[5]*Institute of Astronomy, University of Cambridge, Madingley Road, CB3 0HA Cambridge, UK*
[6]*Kavli Institute for Astronomy and Astrophysics, Peking University, Yi He Yuan Road 5, Hai Dian District, Beijing 100871, China*
[7]*Department of Astronomy, University of California, Berkeley, CA 94720-3411, USA*
[8]*Senior Miller Fellow, Miller Institute for Basic Research in Science, University of California, Berkeley, CA 94720, USA*
[9]*Astronomy Department, California Institute of Technology, Pasadena, CA 91125, USA*
[10]*Tuorla Observatory, Department of Physics and Astronomy, University of Turku, Väisäläntie 20, FI-21500 Piikkiö, Finland*
[11]*Nordic Optical Telescope, Apartado 474, E-38700 Santa Cruz de La Palma, Spain*
[12]*Carnegie Observatories, 813 Santa Barbara Street, Pasadena, CA 91101, USA*
[13]*Astrophysics Research Centre, School of Mathematics and Physics, Queen's University Belfast, Belfast BT7 1NN, UK*
[14]*Institute for Astronomy, University of Hawaii, 2680 Woodlawn Drive, Honolulu, HI 96822, USA*
[15]*Lunar and Planetary Lab, Department of Planetary Sciences, University of Arizona, Tucson, AZ 85721, USA*
[16]*Dark Cosmology Centre, Niels Bohr Institute, University of Copenhagen, Juliane Maries Vej 30, DK-2100 Copenhagen, Denmark*
[17]*Department of Physics and Astronomy, Aarhus University, Ny Munkegade 120, DK-8000 Aarhus C, Denmark*
[18]*Department of Particle Physics and Astrophysics, Faculty of Physics, The Weizmann Institute of Science, Rehovot 76100, Israel*
[19]*Gran Telescopio Canarias (GRANTECAN), Cuesta de San José s/n, E-38712 Breña Baja, La Palma, Spain*
[20]*Instituto de Astrofísica de Canarias, Vía Láctea s/n, E-38200 La Laguna, Tenerife, Spain*
[21]*Institut de Ciències de l'Espai (CSIC - IEEC), Campus UAB, Camì de Can Magrans S/N, E-08193 Cerdanyola (Barcelona), Spain*
[22]*Antelope Hills Observatory, 980 Antelope Drive West, Bennett, CO 80102, USA*
[23]*66 Cours de Lassus, F-66000 Perpignan, France*
[24]*Department of Astronomy, The Oskar Klein Centre, AlbaNova University Center, Stockholm University, SE-10691 Stockholm, Sweden*
[25]*Applied Physics Department, Polytechnic Engineering School of Algeciras, University of Cádiz, Avenida Ramón Puyol S/N, E-11202 Algeciras, Spain*
[26]*Department of Physics and Astronomy, University of Iowa, Iowa City, IA 52242, USA*
[27]*Groupe SNAude France, 364 Chemin de Notre Dame, F-06220 Vallauris, France*
[28]*Dipartimento di Fisica e Astronomia, Università di Padova, via Marzolo 8, I-35131 Padova, Italy*
[29]*Osservatorio Astronomico di Castelmartini, Via Bartolini 1317, I-51036 Larciano, Pistoia, Italy*
[30]*Space Telescope Science Institute, 3700 San Martin Drive, Baltimore, MD 21218, USA*
[31]*Observation and Data Center for Cosmosciences, Faculty of Science, Hokkaido University, Kita-ku, Sapporo, Hokkaido 060-0810, Japan*
[32]*Nayoro Observatory, 157-1 Nisshin, Nayoro, Hokkaido 096-0066, Japan*
[33]*VSOLJ, Nishi juni-jou minami 3-1-5, Nayoro, Hokkaido 096-0022, Japan*

This paper has been typeset from a TEX/LATEX file prepared by the author.